Acta Materialia 248 (2023) 118770

Contents lists available at ScienceDirect

Acta Materialia

journal homepage: www.elsevier.com/locate/actamat

Monovacancy-hydrogen interaction in pure aluminum: Experimental and *ab-initio* theoretical positron annihilation study

Mohamed Elsayed [a,b,*], Torsten E.M. Staab [c], Jakub Čížek [d], Reinhard Krause-Rehberg [a]

[a] Department of Physics, Martin Luther University Halle, 06099 Halle, Germany
[b] Department of Physics, Faculty of Science, Minia University, 61519 Minia, Egypt
[c] Department of Chemistry, University Wuerzburg, LCTM, Roentgenring 11, 97070 Wuerzburg, Germany
[d] Faculty of Mathematics and Physics, Charles University, V Holešovičkách 2, Praha CZ-180 00, Czech Republic

ARTICLE INFO

Keywords:
Positron annihilation spectroscopy
Ab-initio DFT calculations
Aluminum vacancies
Hydrogen-vacancy interaction
Vacancy formation energy

ABSTRACT

We report here on hydrogen-vacancy interactions in high purity aluminum by employing positron annihilation spectroscopy (PAS) analysis of hydrogen-loaded samples, aiming to study the mobility of vacancies. The samples were heat treated at 893 K in an atmosphere consisting of a mixture of H_2 and Ar gas and, thus, loaded with hydrogen. The samples were then quenched to ice water and subsequently measured *in-situ* at different temperatures. In parallel we performed *ab-initio* density functional theory (DFT) calculations of lifetimes of positrons trapped in vacancies associated with 1–8 H atoms. Our experimental results suggest in comparison with the *ab-initio* calculations that complexes of vacancies with one hydrogen atom (V-H pairs) were formed in Al samples annealed in a mixture of H_2 and Ar gas. Furthermore, hydrogen absorbed in aluminum immobilizes vacancies, i.e. the recovery of vacancies is delayed from 220 K up to around 280 K. At that temperature, V-H complexes start to dissociate, and hydrogen atoms previously bound to vacancies are released. In contrast, for Al samples not loaded with hydrogen isolated monovacancies become mobile around 220 K. In both cases mobile vacancies start to form vacancy clusters. From our experimental data we determined that the formation energy of monovacancies in Al is 0.62 ± 0.01 eV. This value is in very good agreement with 0.63 eV obtained by our *ab-initio* DFT calculations.

1. Introduction

Aluminum and its alloys are used in many modern structural and functional materials owing to their superior properties such as lightweight, high strength-to-weight ratio, high thermal conductivity, and good recyclability. The mechanical properties like tensile strength, elongation, fatigue strength of metallic materials are determined by their microstructure, which includes lattice imperfections (defects) like vacancies, dislocations, grain boundaries or precipitates. In particular vacancies and their complexes with hydrogen play a crucial role in embrittlement and crack initiation [1,2].

Vacancies are present in solids at any temperature. However, their concentration in a material in thermal equilibrium is governed by the minimum of the Gibbs free energy and depends via an Arrhenius type law exponentially on temperature. Furthermore, vacancies can be induced into materials by irradiation, deformation, or rapid cooling from elevated temperatures. Such vacancies are called excess or supersaturated vacancies, i.e. their concentration is higher than their expected equilibrium concentration.

Migrating vacancies mediate diffusion of atoms of alloying elements resulting in formation of precipitates [3]. Vacancies may also agglomerate into vacancy clusters, which may grow to larger voids playing a key role in fracture [4]. The coalescence of vacancies is influenced by several factors: their concentration, their migration energy, and their interaction with impurity atoms or dislocations [5].

In the melt and hence, during casting, aluminum and its alloys may contain significantly higher amounts of hydrogen than soluble in the solid state. This can cause problems after solidification due to the formation of hydrogen bubbles, which may act as initiations of cracks [6]. Also an interaction with moisture during further (heat) treatments may lead to an uptake of hydrogen [7]. Another possibility is hydrogen entering fresh metallic surface parts [8] created due to crack propagation under corrosive conditions.

Ab-initio calculations revealed an attractive interaction between

* Corresponding author at: Department of Physics, Martin Luther University Halle, Halle 06099, Germany.
E-mail addresses: mohamed.elsayed@physik.uni-halle.de, melabdalla@yahoo.co.uk (M. Elsayed).

https://doi.org/10.1016/j.actamat.2023.118770
Received 18 April 2022; Received in revised form 31 January 2023; Accepted 6 February 2023
Available online 15 February 2023

vacancies and hydrogen absorbed in interstitial sites [4]. It turns out that in many metals several H atoms can be trapped in a vacancy [4,9–11]. First-principle calculations showed that hydrogen trapping in vacancies occurs also in aluminum [12–16] and underlined the effect of the H trapping in vacancies on reduction of hydrogen diffusion in the Al matrix [4,9,17]. The binding energy of a hydrogen atom in a vacancy in Al is determined experimentally to be about 0.52–0.53 eV [18,19].

Absorbed hydrogen decreases the concentration of „pure“ vacancies in thermal equilibrium and, thus, it looks as if the formation energy would be lowered, which results in a significant increase of the equilibrium concentration of all vacancies: with / without hydrogen [18, 20–22]. Immobilizing hydrogen by trapping into vacancies may prevent its accumulation and, thus, suppress the technological problem of hydrogen-induced embrittlement [1,2]. The most recent study showed that hydrogen leads to delaying the hardening kinetics in Al-Cu alloy owing to the slower growth of GP zones during natural aging, which is explained by hydrogen trapping in vacancies reducing thereby the Cu diffusion coefficient and Al self-diffusion according to the *ab-initio* calculations in [23]. Moreover, Hydrogen trapping in vacancies not only reduces the diffusivity of hydrogen in the Al matrix but also reduces the mobility of vacancies and suppresses their agglomeration into vacancy clusters. For example Zamponi et al. proposed that hydrogen introduced to an AA6013 Al-alloy fatigued under corrosive environment could be responsible for hindering the motion of vacancies at room temperature (RT) [8]. Thus, elucidation of the hydrogen interaction with vacancies is important for understanding the mechanism of hydrogen embrittlement.

Positron annihilation spectroscopy (PAS) is a defect spectroscopy method with a high sensitivity not only to open volume defects such as vacancies or vacancy clusters but also to complexes of these defects with alloying elements in metals or impurities in semiconductors [24–29]. The electronic structure of an isolated vacancy is modified by hydrogen trapping. As a consequence, positron characteristics, e.g. lifetime and annihilation line shape parameters, are changed when a vacancy-hydrogen complex is formed. This makes PAS a suitable tool for studying the hydrogen-vacancy interaction in metals.

While several indirect techniques such as ion beam analysis and electrical resistometry were employed for studying the hydrogen-defect interactions in metals [1,30], there is only one single study [19] employing PAS for the investigation of hydrogen interaction with vacancies in aluminum and its alloys. Furthermore, the decomposition of positron lifetime spectra into individual components was not shown in the study [19], i.e. the effect of hydrogen trapped in Al vacancies on the lifetime of the trapped positron was not determined.

Monovacancies in thermal equilibrium in Al are studied in this work by positron annihilation lifetime (PALS) and Doppler broadening spectroscopy (DBS) as well as coincidence Doppler broadening spectroscopy (CDBS) performed *in-situ* at various temperatures. The vacancy formation energy and entropy were accurately determined. Furthermore, hydrogen interaction with vacancies was investigated and the thermal stability of vacancies and vacancy-hydrogen complexes was compared. PAS investigations were combined with *ab-initio* DFT modeling of vacancies and vacancy-hydrogen complexes.

2. Methods

2.1. Experimental details

A high purity Al (99.9995%) reference material was used in this study. Slices having 10 mm diameter and 1 mm thickness were used for PAS experiments.

To study vacancies in thermal equilibrium the samples were well annealed (823 K/ 2 h) and chemically etched. The annealed samples were measured in the range 300–660 K in vacuum $< 10^{-6}$ mbar.

To study hydrogen-vacancy interaction, the samples were heat treated for 2 h at 893 K under flowing of Varigon H5 gas (a mixture consisting of 5% H_2 and 95% Ar) and then rapidly quenched to ice water in order to freeze most of the thermal vacancies. For this purpose, a vertical quenching furnace is used [28,29], which enables to achieve a quenching rate in the order of 1700 K/s. Hydrogen uptake takes place during heat treatment at high temperatures [31,32]. Accordingly, heating Al at temperatures close to its melting point (e.g. 40 K below its melting point) under a flow of Varigon causes hydrogen uptake and diffusion in the matrix.

If pure Al is quenched to RT and aged at RT for a long time, only vacancy clusters with a density slightly above the PAS detection limit are measured [29]. To avoid aging at RT, the positron source was quickly sealed between quenched samples and the sample-source sandwich was immediately moved into a LN_2 cryostat pre-cooled at 140 K. The estimated period for which the quenched samples were exposed to RT is less than 2 min. The samples were investigated by PAS in the temperature range 80–400 K.

A temperature-controlled digital positron lifetime spectrometer with a time resolution of 170 ps [33,34] was employed. A 25 μCi ^{22}Na positron-source wrapped in a 6 μm Al foil was sandwiched between two identical samples. A source contribution of 16.9% was extracted as described in Ref. [29]. The positron source deposited on the Al foil is used for studying the thermal equilibrium vacancies. Another positron-source wrapped in a 7.5 μm Kapton foil is used for the temperature-dependent measurements. The source contribution of the Kapton foil source is 13.4% with the parameters (382 ps for Kapton foil and 4 ns / 0.65% for glue of the double sticky ring used to close the source).

A total statistics of 4.5×10^6 counts was recorded in each positron lifetime spectrum. The lifetime spectra were analyzed by the program LT9 [35], i.e. decomposed into one or two components convoluted with a Gaussian resolution function, after source and background corrections.

The presence of vacancy defects is indicated by an increase of the average positron lifetime τ_{av}, which is calculated from the resolved lifetime components in accordance with $\tau_{av} = \sum_i^{k+1} I_i \tau_i$. The index i denotes the different lifetime components with individual lifetimes τ_i and corresponding intensities I_i. The index k stands for the number of different defect types, where positrons are trapped. This leads to k+1 components in the positron lifetime spectrum. τ_{av} is a very sensitive parameter and changes in the order of 1 ps can be accurately detected.

Open volume defects in Al samples were characterized also using the CDBS technique. The CDBS measurements were done using a digital spectrometer in the so-called semi-digital mode, as described in the references [36,37]. The CDBS spectrometer is described in more detail in Ref. [28]. Results of CDBS measurements are presented as ratio curves with respect to a well annealed Al reference.

2.2. Ab-initio calculations

Electronic structure calculations were carried out within the density function theory implemented in the Viena *ab-initio* simulation package (VASP) [38,39]. The theoretical approach used in the present work is very similar to that employed in Ref. [29]. We used plane augmented wave (PAW) potentials, 500 eV energy cut-off, and Fermi smearing of the electronic occupancy. Defects were modeled using 108 atom based supercells consisting of $3 \times 3 \times 3$ fcc unit cells with the lattice parameter $a = 4.041$ Å obtained by VASP structure optimization. Equilibrium geometries of defects were determined by fully relaxing ion positions and the supercell volume. The Brillouin zone was sampled using a $8 \times 8 \times 8$ k-point mesh generated applying the Monkhorst-Pack scheme [40]. Convergence tests revealed that calculated energies are converged within ~ 0.01 eV.

Since hydrogen is a light atom, the vibration energy of H ions in the Al lattice has to be considered. The zero-point energy (ZPE) of hydrogen was calculated using the Einstein model for localized H modes, i.e. by summing up the vibration energies of hydrogen normal modes, $ZPE = \frac{1}{2}\sum_i h\nu_i$, where h is the Planck constant [10]. The vibration frequencies ν_i

were determined from the energy versus displacement curves of H atoms. The vibrational energies of Al atoms are assumed to be negligible compared to that of H atoms.

The fcc Al lattice contains tetrahedral (T) and octahedral (O) interstitial sites. *Ab-initio* calculations revealed that hydrogen absorbed in the Al lattice occupies preferentially T sites and causes outward relaxation of the four neighboring Al ions with a displacement of 0.13 Å in the direction away from the H ion. Although H prefers T sites, the difference of the potential energy of H located in T and O sites is rather small, ≈ 0.05 eV only. The formation energy of hydrogen interstitials (H_i) in the Al lattice was calculated from the expression [10,41–43]

$$E_{F,H_i} = E_{cell}[H_i] - \left(E_{cell}[bulk] + \frac{1}{2}E[H_2]\right), \quad (1)$$

where $E_{cell}[H_i]$ is the total energy of a super-cell containing H_i located in a T site, E_{cell}[bulk] is the total energy of a perfect (defect-free) super-cell, and $E[H_2]$ is the energy of the H_2 molecule. The ZPE contributions of hydrogen vibrations are included in the energies $E_{cell}[H_i]$ and $E[H_2]$.

The vacancy formation energy was calculated using the equation [10,41–43],

$$E_{F,V} = E_{cell}[V] - \frac{N-1}{N}E_{cell}[bulk], \quad (2)$$

where E_{cell}[V] is the total energy of a super-cell containing a vacancy V and $N = 108$ is the number of Al atoms in a perfect super-cell.

To get information about the hydrogen interaction with a vacancy, the binding energy $E_{B,V\text{-}H}$ of interstitial H to a vacancy was calculated from the expression [10,41–43]

$$E_{B,V-H} = E_{cell}[V] + E_{cell}[H_i] - (E_{cell}[V-H] + E_{cell}[bulk]), \quad (3)$$

where E_{cell}[V-H] is the total energy of a super-cell containing a vacancy associated with one hydrogen atom (V-H complex). Note that a positive value of the binding energy $E_{B,V\text{-}H}$ indicates that the formation of V-H is energetically favorable, i.e. the V-H complex has lower energy than an isolated vacancy and H_i.

A vacancy can be associated with multiple H atoms [10,42,43]. The formation energy of a complex consisting of a vacancy associated with n H atoms (V-nH complex) can be calculated from the expression [10, 41–43]

$$E_{F,V-nH} = E_{cell}[V-nH] - E_{cell}[bulk] + \mu_{Al} - n\mu_H \quad (4)$$

where E_{cell}[V-*n*H]is the total energy of the supercell containing a V-nH complex including the ZPE of H atoms and μ_{Al}, μ_H represent the chemical potential of Al and H atoms, respectively. One has to distinguish the formation energy of a V-nH complex in (i) pure Al and (ii) Al containing already absorbed hydrogen. In the present work we consider formation of V-nH complexes in the pure Al lattice, i.e. the case (i), because hydrogen solubility in the Al lattice is very low [44]. The formation of a V-nH complex requires the creation of a vacancy in the Al lattice and absorption of nH atoms. Hence, the chemical potential for an Al atom is $\mu_{Al} = E_{cell}[bulk]/N$ and the chemical potential for the H atom is $\mu_H = E[H_2]/2$, where $E[H_2]$ is the calculated energy for H_2 molecule. Inserting the chemical potentials into Eq. (4) one gets the formation energy of V-nH complex

$$E_{F,V-nH} = E_{cell}[V-nH] - \left(\frac{N-1}{N}E_{cell}[bulk] + \frac{n}{2}E[H_2]\right). \quad (5)$$

Note that in the case (ii), i.e. considering the formation energy of V-nH in the Al lattice containing already absorbed hydrogen atoms in tetrahedral sites the chemical potential of hydrogen atoms can be calculated as $\mu_H = E_{cell}[H_i]$-E_{cell}[bulk] and the formation energy of the V-nH complex will be $E_{F,V-nH} - nE_{F,H_i}$. However, because of very low hydrogen solubility in Al under the conditions of the present experiment (annealing in the Varigon H5 gas) realistic conditions correspond to case (i) and the formation energy of the V-nH complex is given by Eq. (5).

The binding energy of a V-nH complex can be calculated as [10,42, 43]

$$E_{B,V-nH} = E_{F,V} + nE_{F,H_i} - E_{F,V-nH}. \quad (6)$$

Positive values of $E_{B,V\text{-}nH}$ indicate that the formation of V-nH complexes is energetically favorable. In order to examine the binding of individual H atoms to a vacancy one can calculate the difference of binding energies

$$\Delta E_{B,n} = E_{B,V-nH} - E_{B,V-(n-1)H}, \quad (7)$$

which gives the energy released when V-(n-1)H is transformed into V-nH complex, i.e. the energy released during the reaction V-(n-1)$H + H_i \rightarrow$ V-nH.

Positron lifetimes were calculated using density functional theory. The ground state positron density was calculated within the so-called standard scheme [45]. In this approximation, the positron density is vanishingly small everywhere and does not affect the bulk electron structure. At first, the electron density *n* in the material is solved without the positron. Subsequently, the effective potential for a positron is constructed as:

$$V_+(\mathbf{r}) = \phi(\mathbf{r}) + V_{corr}[n, \nabla n], \quad (8)$$

where $\phi(r)$ is the Coulomb potential produced by the charge distribution of electrons and nuclei and V_{corr} is the zero positron density limit of the electron-positron correlation potential [45]. The ground state positron wave function $\psi_+(\boldsymbol{r})$ and the positron ground state energy eigenvalue E_+ were calculated by solving the single-particle Schrödinger equation:

$$-\frac{1}{2}\nabla^2\psi_+(\mathbf{r}) + V_+(\mathbf{r})\psi_+(\mathbf{r}) = E_+\psi_+(\mathbf{r}). \quad (9)$$

The positron lifetime τ was calculated from the overlap of the electron density $n(\boldsymbol{r})$ and the positron density $n_+(\mathbf{r}) = |\psi_+(\mathbf{r})|^2$ using the expression:

$$\tau = \left\{\pi r_e^2 c \int n_+(\mathbf{r})n(\mathbf{r})\gamma[n]d\mathbf{r}\right\}^{-1}, \quad (10)$$

where r_e is the classical electron radius and c is the speed of light. The electron enhancement factor γ accounts for the pile-up of electrons at the positron site [45]. The electron-positron correlation potential and the enhancement factor were treated within the local density approximation (LDA) using the parametrization by Boronski and Nieminen [46]. Brillouin-zone integration over the lowest-lying positron state [47] was used in calculations of positron density for vacancies to achieve rapid convergence of the results with respect to the supercell size. Positron calculations were performed using relaxed geometries of defects obtained from VASP. For calculations of the positron density, the supercells used in VASP were enveloped by a perfect lattice to get larger supercells consisting of 256 atoms.

The momentum distribution of the annihilating electron-positron pairs was calculated within the two-component DFT using the approach described in Ref. [48] as implemented in the ABINIT code (version 9.6.2) [49]. The momentum distribution of annihilating electron-positron pairs is described by the expression [50]

$$\rho(\mathbf{p}) = \pi r_e^2 c \sum_j \gamma_j \left| \int e^{ipr}\psi_+(\mathbf{r})\psi_j(\mathbf{r})d\mathbf{r}\right|^2, \quad (11)$$

where ψ_j (r) represents the electron wave functions and the sum runs over all occupied electron states. The state-dependent enhancement factor γ_j [51] accounts for the correlation effects for each electronic state

$$\gamma_j = \int n_+(\mathbf{r})n_j(\mathbf{r})\gamma[n, \nabla n]d\mathbf{r} \Big/ \int n_+(\mathbf{r})n_j(\mathbf{r})d\mathbf{r}. \quad (12)$$

The contribution of the core and the valence electrons to the momentum distribution was calculated separately. The contribution of core electrons was obtained using the core electron wave-function of isolated atoms (frozen core approximation). The contribution of valence electrons was calculated using valence electron wave functions determined by ABINIT using the PAW method. The generalized gradient approximation (GGA) functional proposed by Barbiellini et al. [52] was used for description of electron-positron correlation effects in the momentum distribution calculations. Note that the momentum distribution calculated using the GGA approach is in better agreement with experiment compared to the LDA functional which slightly overestimates annihilations with core electrons [51]. To ensure the completeness of PAW dataset 2s and 2p states have been considered as valence electrons resulting in 11 valence electrons and 2 core electrons for Al. The corresponding PAW potentials were calculated using the ATOMPAW code (version 4.2) [53]. The calculated momentum distribution was convoluted with a Gaussian having a FWHM of 2.25×10^{-3} $m_o c$ in order to mimic the finite energy resolution of the detector. The calculated momentum distributions are presented as ratio curves related to the perfect (defect-free) Al.

3. Results and discussion

3.1. Ab-initio calculations

Fig. 1 shows the density of a positron delocalized in a defect-free Al lattice and in an Al lattice containing an interstitial H atom (H_i), trapped in a single vacancy, and in a vacancy-H atom complex. We carried out *ab-initio* calculations to determine lifetimes of the positron delocalized in a perfect lattice (bulk) and trapped at various defects. Results are listed in Table 1.

The positron density calculated in the (001) plane is plotted in Fig. 1. The positron in a perfect (defect-free) Al lattice is delocalized as a modulated Bloch-like wave, see Fig. 1(a), and the calculated bulk positron lifetime of 167 ps is in good agreement with literature [16,29,54]. *Ab-initio* calculations performed in the present work revealed that it is energetically favorable for hydrogen in the Al lattice to occupy T sites. However, the energy difference between T sites and O sites is rather small, 0.05 eV only. Experimental results of hydrogen-implanted Al using channeling and nuclear reaction analysis confirmed that all the implanted hydrogen occupies T sites [55]. The formation energy of interstitial hydrogen (H_i) calculated using Eq. (1) $E_{F,Hi}$= 0.7 eV is in very good agreement with the value of 0.71 eV calculated by Nazarov et al. [56] and is also in reasonable agreement with experimental values of dilute hydrogen's heat of solution reported in the literature [57–60]. Hydrogen absorption in interstitial sites of the Al lattice is an endothermic process ($E_{F,Hi}> 0$) in accordance with the fact that hydrogen solubility in the fcc Al lattice is practically zero [61].

The positron remains delocalized also in the lattice containing interstitial H atom, see Fig. 1(b). However, from comparison of Fig. 1(a) and (b) one can notice that while in the perfect lattice the positron density is the same in all O sites in the lattice containing H_i the positron density is slightly enhanced in O sites adjacent to H_i, see arrows in Fig. 1

Table 1
Calculated formation energies (E_F) and positron lifetimes (τ) for various defects as well as the lifetime of free positrons delocalized in the perfect Al lattice (bulk). The calculations were done in the relaxed geometry.

Defect	E_F (eV)	τ (ps)
Bulk-Al		167
H interstitial (T-site)	0.70	167
Vacancy	0.63	237
Vacancy-H complex (V-H)	0.96	225
Divacancy	1.20	257
Divacancy-H complex (2V-H)	1.55	248
Divacancy-2H complex (2V-2H)	1.78	244

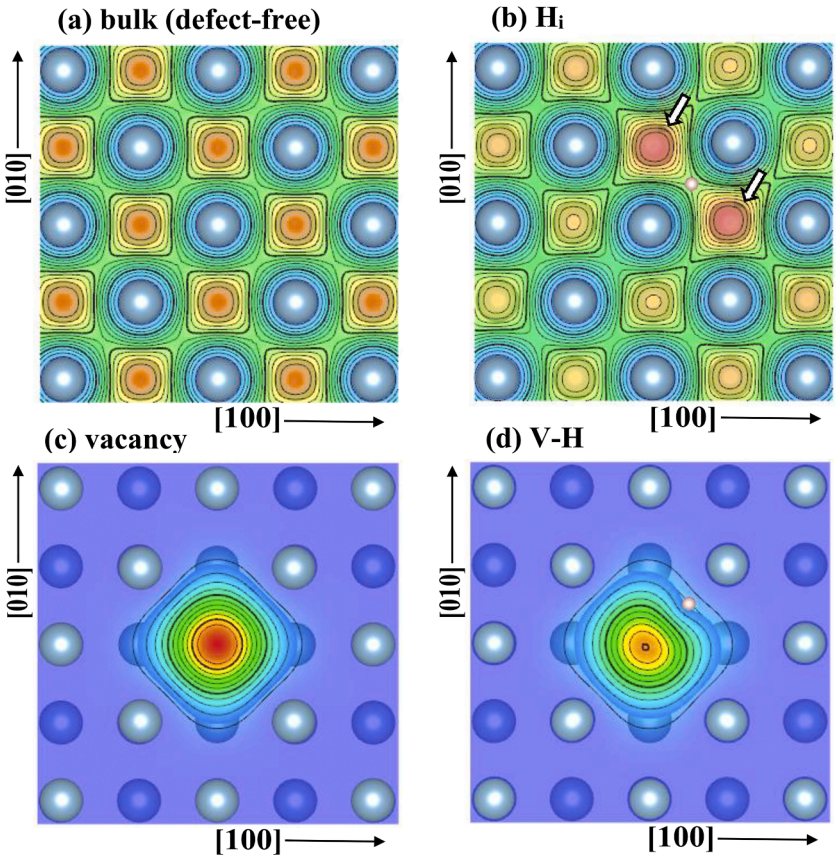

Fig. 1. Atomic configuration and calculated positron density in the (001) plane: (a) a perfect (defect-free) lattice, (b) H atom in tetrahedral interstitial position, arrows indicate O sites adjacent to H_i where the positron density is slightly enhanced; (c) isolated vacancy, (d) vacancy associated with one H atom. Large spheres indicate Al, where bright circles indicate Al ions located in the (001) plane while dark circles are Al ions located below the (001) plane. The small sphere refers to the H atom, which is located 0.89 Å above the (001) plane.

(b). This is caused by the fact that the open volume of these O sites is slightly enhanced due to the outward relaxation of Al ions around H_i and local accumulation of negative charge around the H atom. However, the perturbation of the positron density in the vicinity of H_i is rather small and the calculated positron lifetime remains practically the same as the bulk value of 167 ps. Hence, H_i is in practice 'invisible' for positrons.

An H atom associated with a vacancy is positioned aside from the vacancy, as clearly shown in Fig. 1(d). Hence, a vacancy associated with an H atom is capable of positron trapping as well, while the positron density becomes asymmetric, since a part of the open space on one side is occupied by the H atom. The presence of the H atom results in a higher electron density and, thus, in a reduced lifetime of the trapped positron of 225 ps.

For comparison, the calculated positron density for an isolated vacancy is plotted in Fig. 1(c). The positron is well localized in the vacancy and the calculated lifetime is 237 ps. The calculated vacancy formation energy using Eq. (2) $E_{F,V} = 0.63$ eV agrees very well with the calculations of Freysoldt et al. [41] done with DACAPO using the GGA scheme giving 0.63 eV and Kohlbach et al. [54] employing the SIESTA code within the LDA scheme, which gave $E_F = 0.64$ eV.

The binding energy of hydrogen to a vacancy calculated using Eq. (3) gives $E_{B,V\text{-}H} = 0.53$ eV. This value is in good agreement with effective medium theory calculations by Larsen and Norskov [62], DFT *ab-initio* calculations by Wolverton et al. [9] as well as with experimental results [19,63]. A positive value of the binding energy testifies an attractive interaction between hydrogen and vacancies, i.e. the V-H complex is energetically more favorable than an isolated vacancy and H_i. The lowest energy configuration of the V-H complex is plotted in Fig. 1(d). Our calculations show that the H atom is located on a line connecting the vacancy and the nearest neighbor T site and is displaced 0.20 Å from the T site towards the vacancy, see Fig. 1(d). Hence, the distance of the H atom from the center of the vacancy is 1.55 Å. This geometry of the V-H complex is in good agreement with *ab-initio* calculations by Wolverton et al. [9]. The formation energy $E_{F,V\text{-}H} = 0.96$ eV for the V-H complex is calculated using Eq. (5).

However, the Al vacancy is found to be capable of trapping multiple H atoms forming V-nH complexes. Various configurations of V-nH complexes were examined and the lowest energy geometry of each complex has been determined. H atoms are found to be located close to the T sites in the lowest energy configuration of the V-nH complexes. Since there are eight T sites surrounding the vacancy, the lowest energy configurations of V-nH complexes corresponding to $n = 1, \ldots, 8$ were calculated and are plotted in Fig. 2. Calculated positron densities in the (001) plane for V-2H, V-4H, V-6H, and V-8H complexes are shown in Fig. 3. The positron is obviously localized in V-nH complexes. The positron density in the vicinity of H ions is diminished due to the Coulomb repulsion between the positron and the positively charged H ions. It results in cut-outs of the positron density in the vicinity of H ions which are clearly visible in Fig. 3.

Fig. 4(a) shows the effect of nH associated with a vacancy on the positron lifetime. The lifetime of positrons trapped in V-nH complexes gradually decreases with an increasing number of H atoms decorating the vacancy due to the increase of electron density in the V-nH complex, which results in an enhancement of the annihilation probability at the vacancy site, decreasing thereby the positron lifetime. The formation energies calculated using Eq. (4) are plotted in Fig. 4(b). With an increasing number of H atoms surrounding the vacancy, the formation energy of the V-nH complex increases because H absorption in the Al lattice is an endothermic process and the formation of the V-nH complexes requires absorption of multiple H atoms. From an inspection of Fig. 4(c) it is clear that the total binding energy $E_{B,V\text{-}nH}$ increases with an increasing number of H atoms. The binding energy $\Delta E_{B,n}$ of the n-th H atom to the V-nH complex calculated using Eq. (7) is plotted in Fig. 4(c) as well and decreases from 0.52 eV down to a value around 0.34 eV for $n \geq 4$. Hence, binding of additional H atoms in V-nH complex becomes weaker with an increasing number of H atoms. Positive values of $\Delta E_{B,n}$

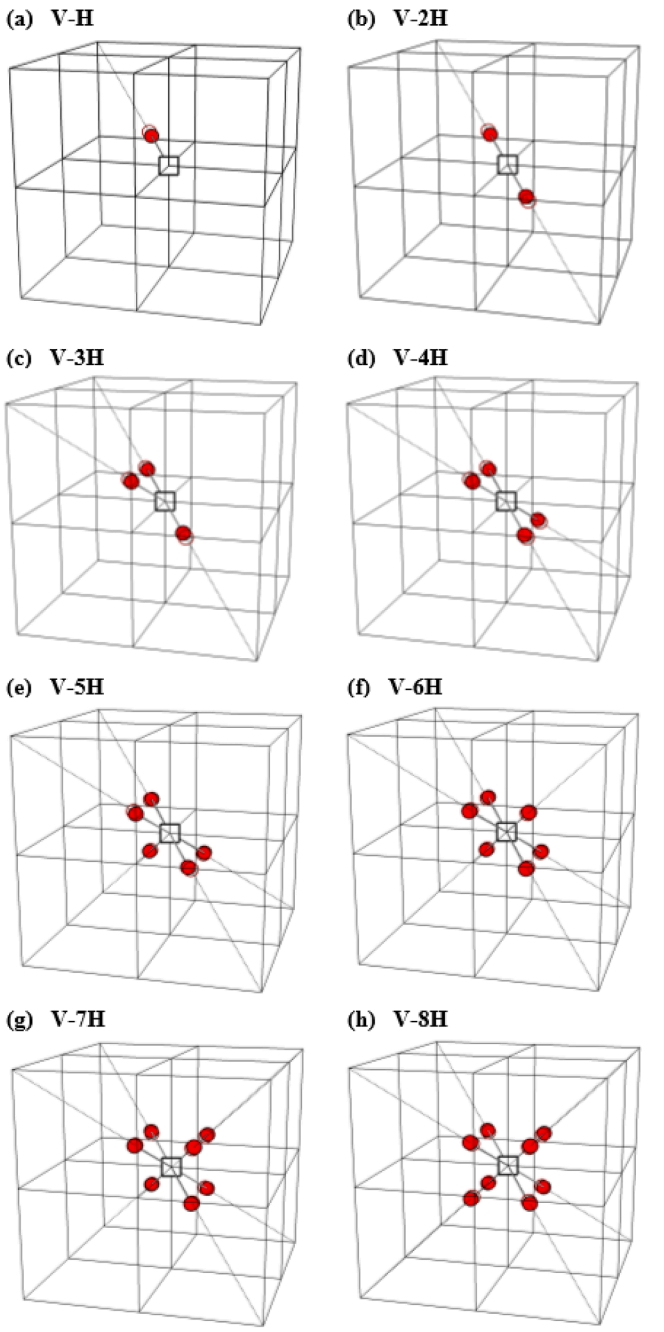

Fig. 2. Lowest energy configurations of V-nH complexes for $n = 1, \ldots, 8$. The vacancy is indicated by a square. H atoms in relaxed configurations are presented by closed red circles; initial non-relaxed positions of H atoms are indicated by open circles.

up to $n = 8$ testify that a vacancy in Al is able to trap up to 8 H atoms in accordance with the calculations by Lu and Kaxiras [4]. This means that H atoms (up to 8) associated with the vacancy have a lower energy than the corresponding number of H atoms located in interstitial sites.

A complex of divacancy and hydrogen was considered as well. The lowest energy configuration of a divacancy associated with one H atom (2V-H complex) and a divacancy associated with two H atoms (2V-2H complex) is shown in Fig. 5(a) and (b), respectively. Similarly to a monovacancy-H complex, H atoms are located close to the nearest neighbor T sites and are slightly displaced towards the vacancy. The formation energy and positron lifetime for 2V-H and 2V-2H complexes are listed in Table 1. Note that the formation energy of the 2V-2H

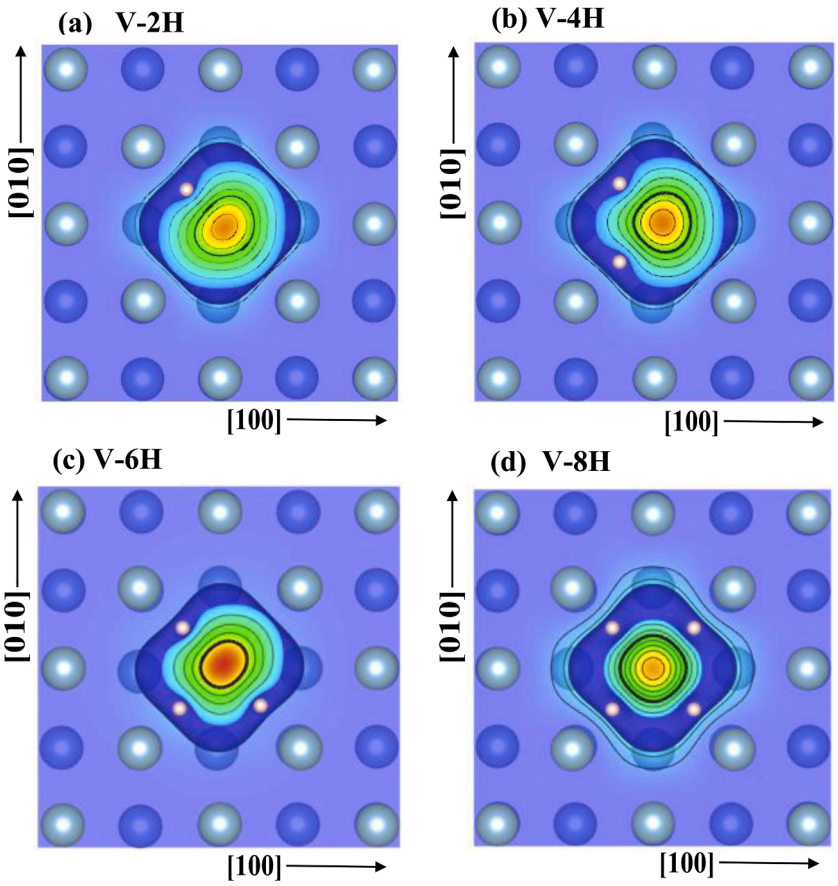

Fig. 3. Atom configurations and calculated positron densities in the (001) plane for (a) V-2H; (b) V-4H; (c) V-6H; (d) V-8H. Large spheres indicate Al atoms. Bright circles indicate Al ions located in the (001) plane while dark circles are Al ions located below the (001) plane. Small spheres represent H atoms located above the (001) plane. Note that there are additional H atoms located below those shown in the figure.

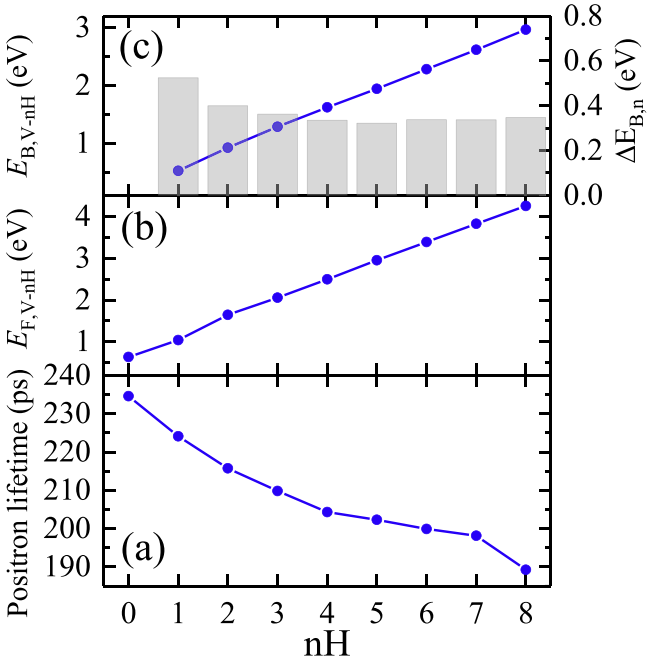

Fig. 4. (a) Calculated lifetime of positrons trapped in a vacancy associated with nH atoms plotted as a function of the number of H atoms nH decorating the vacancy; (b) The total formation energy of V-nH complexes; (c) The binding energy of the V-nH complex $E_{B,V\text{-}nH}$ (points) and the binding energy of the last H atom $\Delta E_{B,n}$ (vertical bars).

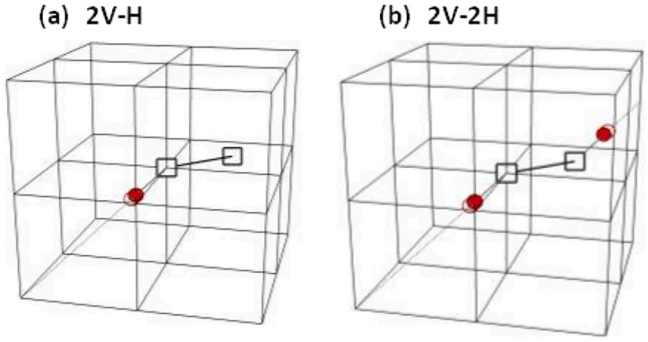

Fig. 5. The lowest energy configurations of a divacancy associated with hydrogen atoms (a) 2V-H complex, (b) 2V-2H complex. Vacancies are indicated by squares. H atoms in relaxed configurations are presented by closed red circles; initial non-relaxed positions of H atoms are indicated by open circles.

complex is slightly lower than twice the formation energy of the V-H complex. Hence, it is energetically favorable for V-H complexes to merge into 2V-2H.

3.2. Thermal equilibrium monovacancies

3.2.1. Positron lifetime spectroscopy

Vacancies in pure aluminum were studied under thermal equilibrium conditions in order to get a clear insight into their properties such as the characteristic defect-related positron lifetime and their formation energy. The results of temperature-dependent positron lifetime measure-

ments of pure Al are displayed in Fig. 6. At RT the sample showed only a single component spectrum with a positron lifetime of (158±1) ps corresponding to positron annihilation in the defect-free Al lattice (so-called defect-free bulk positron lifetime τ_b). This value agrees well with the literature where τ_b in the range 158–163 ps has been reported [64–69]. With increasing temperature, the average positron lifetime increases very slightly (~2 ps/100 K) in the temperature range up to 450 K. This can be ascribed to thermal lattice expansion. Using the coefficient of linear thermal expansion of $23.1 \times 10^{-6}\,K^{-1}$ for Al [70] one can calculate that the increase of the bulk positron lifetime due to thermal expansion of the Al lattice is 1 ps/100 K. At $T > 500$ K τ_{av} strongly rises, indicating an increase in the concentration of thermal equilibrium vacancies above the detection limit for PAS. At $T > 500$ K the spectra can be reliably decomposed into two components: (i) a contribution with lifetime τ_1 corresponding to positrons annihilating in the free state, (ii) a component with the lifetime $\tau_2 = \tau_d = (240 \pm 2)$ ps which stems from positrons trapped at defects. The τ_2 value remains constant, see Fig 6, and agrees very well with the lifetime of 237 ps of positrons trapped at vacancies obtained from *ab-initio* calculations, see Table 1. Our measured value of $\tau_2 = 240$ ps is very close to $\tau_2 = 237 \pm 3$ ps obtained at 700–900 K for pure Al [69], where a ^{22}Na source was directly deposited on the sample, and also to 244 ps obtained at $T > 620$ K in Ref. [71]. However, other earlier measurements showed $\tau_2 = 251 \pm 3$ ps for a monovacancy [66], which is distinctly higher than our experimental and calculated values. The intensity I_2 clearly increases reaching about 70% at 610 K, reflecting an increase in the concentration of vacancies. The lifetime τ_1 is less than the Al bulk lifetime value and decreases with increasing measurement temperature owing to an increase of the vacancy concentration according to the simple trapping model. The τ_1 value calculated from the decomposed lifetime parameters according to the simple trapping model ($\tau_1 = \tau_b \frac{\tau_d - \tau_{av}}{\tau_d - \tau_b}$) is very close to the measured one, indicating that the assumptions of the simple trapping model are fulfilled in the present case. τ_1 significantly decreases with the measurement temperature owing to an increase of the vacancy concentration.

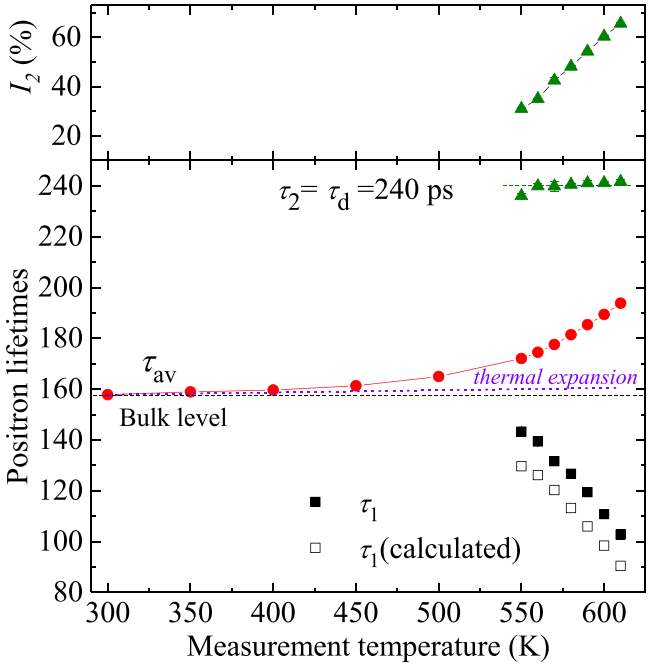

Fig. 6. Results of positron lifetime spectra decomposition of the pure Al sample measured in the temperature range 300–610 K. A two-component fitting of the spectra was employed whenever possible. The defect-related lifetime τ_2 (triangles) and the reduced bulk lifetime τ_1 (squares) as well as the average lifetime τ_{av} are displayed in the lower panel, while the intensity I_2 is shown in the upper panel. Open squares represent τ_1 values calculated from the spectra decomposition according to the simple trapping model. The dashed line indicates the calculated increase of the average positron lifetime caused by thermal expansion of the Al lattice.

It has been reported that electron irradiation induced monovacancies into Al exhibit a positron lifetime of 238±6 ps with an intensity of only 22% in the low temperature range up to 220 K [69]. Whereas annealing of this sample led to monovacancy migration and formation of vacancy clusters at RT with a lifetime of 300 ps typical for vacancy clusters [69].

When the measurement was finished the sample temperature was slowly decreased down to RT and a repeated measurement of the sample showed a single component spectrum with the bulk positron lifetime value of 158 ps. This confirms that vacancies generated at high temperatures are thermal equilibrium vacancies that disappear when the sample is slowly cooled down to RT.

In-situ temperature dependent Doppler broadening measurements of an Al sample were performed as well and results are presented in the Supplementary material (Section S1). Results of Doppler broadening investigations are in accordance with positron lifetime spectroscopy. The temperature dependence of the *S* parameter is similar to that of the mean positron lifetime and an *S-W* plot confirmed the existence of one kind of defects, namely monovacancies.

Variable energy positron annihilation spectroscopy (VEPAS) [72] was employed to check for possible oxidation of the Al sample at elevated temperatures. Results of the VEPAS investigations are presented in the supplementary material (Section S3). The VEPAS characterization of the Al sample after *in-situ* PALS measurement at various temperatures up to 660 K revealed that the sample is covered only by a very thin (12.7 nm) oxide layer on the surface which has no influence on our PAS results.

3.2.2. *Coincidence Doppler broadening spectroscopy*

In-situ CDBS measurements performed at 650 K resulted in the ratio curve plotted in Fig. 7. The momentum distributions for comparison were calculated for the relaxed geometries of an isolated vacancy and a divacancy in Al. Their ratio curves with respect to the momentum distribution calculated for perfect (defect-free) Al are plotted in Fig. 7 as well. The calculated ratio curve of the divacancy is distinctly below the measured curve over the whole momentum range, meaning that the defect type observed in the experiment cannot be a divacancy. On the other hand, the measured ratio curve is very similar to the calculated curve for a monovacancy. This confirms the interpretation of our lifetime results and proves that monovacancies are formed in thermal

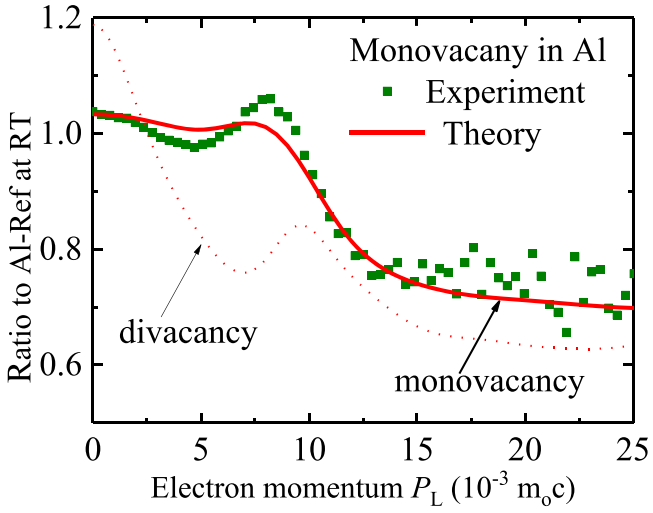

Fig. 7. CDBS ratio curve normalized to defect-free Al measured *in-situ* in pure Al at 650 K together with the calculated ratio curves for a vacancy (solid line) and a divacancy (dotted line) in relaxed geometry.

equilibrium in the considered temperature range.

3.2.3. Monovacancy formation energy

The concentration of vacancies can be calculated according to the equation

$$C = \exp(S_F / k_B)\exp(-E_F / k_B T) \quad (13)$$

where k_B is the Boltzmann constant and S_F stands for the vacancy formation entropy. The equilibrium concentration is calculated as a function of temperature for monovacancies and divacancies in Al using E_F values obtained from *ab-initio* calculations given in Table 1. $S_F = 1.03\ k_B$ and $S_F = 2.04\ k_B$ were employed in the calculations for monovacancies and divacancies, respectively.

As shown in Fig. 8, the concentration of monovacancies is significantly higher (by 6 orders of magnitude at 400 K and by 2 orders of magnitude at 900 K) than that of divacancies. This further supports the observation of just monovacancies in the temperature range 400–900 K. One can see in Fig. 8 that monovacancies are present at RT in a very low concentration, which is beyond the lower sensitivity limit of PAS.

Even though the vacancy formation energy in aluminum has been studied extensively both experimentally and theoretically a large spread of values exists. The values for the vacancy formation energy in the literature [69,71,73–76] fall into the range from 0.61 to 0.82 eV, see Table 2. For example, the formation energy of 0.71–0.82 eV was obtained from fitting the positron lifetime data depending on various fixed parameters in the data fitting process [69]. These values are somewhat higher than values obtained in other studies. Another study showed a formation energy range of 0.60–0.70 eV depending on the way of fitting of Doppler broadening data [77]. A formation energy of 0.65 eV was obtained from a positron study but the lifetime analysis is not shown [68]. It should be noted that most of previous PAS studies did the data treatment under certain assumptions such as assuming τ_d constant, see for example [71] and references therein.

In contrast to previous PAS studies all parameters are left free in our data treatment and we applied a simple method, which is independent of either the value of the positron trapping coefficient or complicated numerical analysis of the data obtained from fitting the spectra. We just applied the two state simple trapping model to calculate the positron trapping rate to vacancies from data of positron lifetime and Doppler broadening measurements performed *in-situ* at various temperatures. The trapping rate κ is calculated according to the expression $\kappa(T) = \frac{1}{\tau_b}\frac{\tau_{av}(T)-\tau_b}{\tau_d-\tau_{av}(T)}$, where $\tau_b = 158$ ps is the bulk positron lifetime measured in defect-free Al at RT, $\tau_d = \tau_2$ is the lifetime of positrons trapped at vacancies and τ_{av} is the average positron lifetime obtained from the decomposition of the lifetime spectra (shown in Fig. 6). Note that the average positron lifetime was used instead of intensities of the components since it is a more robust parameter being insensitive to mutual correlation of fitting parameters. Using the results of Doppler broadening spectroscopy (Fig. S1) the positron trapping rate to vacancies can be calculated applying the relation $\kappa(T) = \frac{1}{\tau_b}\frac{S(T)-S_b}{S_d-S(T)}$, where $S(T)$ is the S parameter measured at temperature T. S_b is the S parameter of defect-free Al reference (measured at RT) and S_d is the S parameter corresponding to positrons trapped in vacancies. Fig. 9 shows the Arrhenius plot of the trapping rate obtained both from the positron lifetime (left part) and Doppler broadening results (right part).

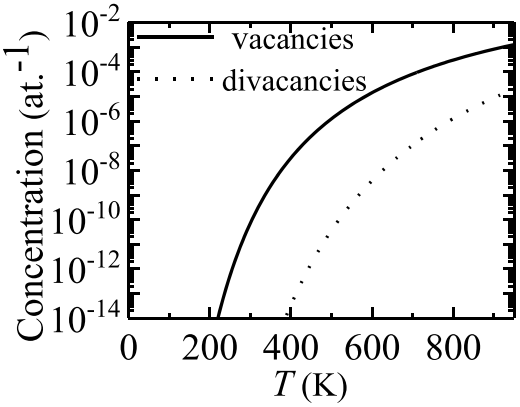

Fig. 8. Thermal equilibrium concentration of monovacancies and divacancies calculated using Eq. (13). $E_F = 0.63$ and 1.2 eV were applied for monovacancies and divacancies, respectively.

Table 2
Formation energies of monovacancies in Al determined experimentally and theoretically in this work in comparison with data from the literature. The approach used for the electron exchange functional, i.e. LDA, GGA possibly with the surface energy correction (SEC) or meta-GGA, and the code used for calculations are given in the table as well.

Vacancy formation energy (eV)			
Experiment		Theory	
0.62 ± 0.01	present work	0.63 - VASP - GGA	present work
0.71 ± 0.05	[69]	0.64 - SIESTA- LDA	[54]
0.69± 0.03	[74]	0.63 - DACAPO - GGA	[41]
0.77	[75]	0.68 - DACAPO - LDA	[41]
0.60 … 0.82 most probable = 0.67 ± 0.03	[76]	0.54 - VASP - GGA	[81]
0.64 ± 0.04	[77]	0.76 - VASP - GGA-SEC	[81]
0.62 ± 0.02	[64]	0.70 - VASP - LDA	[81]
0.62 ± 0.02	[73]	0.69 - VASP - LDA-SEC	[81]
0.65	[68]	0.55 - LDA	[82]
0.62	[83]	0.71 - VASP - LDA	[84]
0.68 ± 0.03	[66]	0.65 - VASP - GGA	[84]
0.61 ± 0.03	[85]	0.77 – VASP-meta-GGA	[82]
0.66 ± 0.02	[71]		

The positron trapping rate to vacancies is governed by the Arrhenius equation $\kappa(T) = \mu C(T) = \mu_{1V}\exp(S_F/k_B)\exp(-E_F/k_B T)$, where C is the equilibrium vacancy concentration, and μ_{1V} is the positron trapping coefficient for monovacancies. Hence, the vacancy formation energy E_F can be obtained from the Arrhenius plot ($\ln\kappa = \text{constant} - E_F/k_B T$). The Arrhenius plot ($\ln\kappa$ versus $1/k_B T$) should be a straight line with the slope -E_F. Fitting of both positron lifetime and Doppler broadening results yields the same slope corresponding to a vacancy formation energy of $E_F = (0.62 \pm 0.01)$ eV. In addition, the vacancy formation entropy S_F can be determined from the Arrhenius plot, where the intercept is $(\ln(\mu_{1V}) + S_F/k_B)$. Employing the positron trapping coefficient $\mu_{1V} = 2.5 \times 10^{14}\ s^{-1}$ for monovacancies in pure Al [69,78], both Doppler broadening and lifetime results give the same value of the vacancy formation entropy $S_F = (1.03 \pm 0.01)\ k_B$. It is worth to note that only a few experimental data on the vacancy formation entropy were reported in the literature. The value $S_F = 1.03\ k_B$ in the present work agrees well with $S_F = 1.1\ k_B$ measured using differential dilatometry [79] and falls into the range 0.9 - 1.2 k_B obtained by *ab-initio* calculations [80,81].

Note that our experimental value $E_F = (0.62 \pm 0.01)$ eV has a rather low uncertainty for both the two independent experimental techniques (positron lifetime spectroscopy and Doppler broadening) applied. Both yielded virtually the same values of vacancy formation energy. Moreover, our experimental value is in excellent agreement with the *ab-initio* calculations described in the present paper yielding $E_F = 0.63$ eV.

Experimental and theoretical E_F values reported in literature are collected in Table 2. The experimental values reported in literature fall into the range from 0.60 to 0.82 eV and their spread is characterized by the standard deviation of 0.05 eV. Taking into account experimental uncertainties of the values reported in literature and listed in Table 2 one

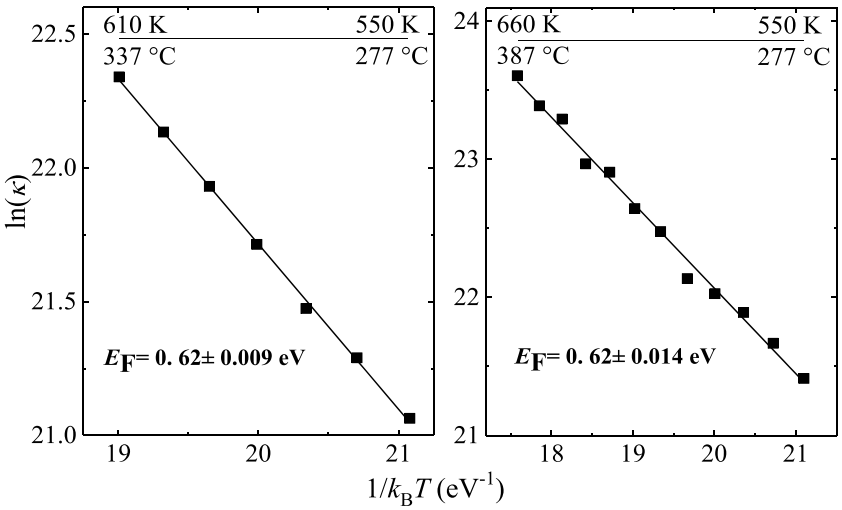

Fig. 9. Arrhenius plots of the trapping rate to thermal equilibrium vacancies in pure Al obtained from the positron lifetime (left panel) and Doppler broadening (right panel) measurements. The solid line represents a linear fit to the experimental data giving the vacancy formation energy E_F = (0.62 ± 0.01) eV.

can calculate the weighted average as

$$E_{F,mean} = \frac{\sum_i \frac{E_{F,i}}{\sigma_i^2}}{\sum_i \frac{1}{\sigma_i^2}}, \quad (14)$$

where σ_i is the uncertainty of the experimental value $E_{F,i}$. Note that in cases when experimental uncertainty was not given in the original paper as in Refs. [68,75,83], it was estimated as 5 times the last significant digit of reported values. In the case when a range of E_F values was reported [76] we used the arithmetical average and the error was estimated by standard deviation. The weighted average calculated by Eq. (14) is $E_{F,mean}$ = (0.64 ± 0.01) eV and it is comparable (within 2 standard deviations) with our experimental value.

It must be mentioned that aluminum as a simple metal is often used as a model system for testing various approaches in computational materials science. Carling et al. [81] showed that a surface energy error correction improves the agreement of E_F calculated within the GGA approach with experiment. Since the time of their publication various approaches for the surface energy correction have been developed [86–89]. The surface energy correction is included in newer meta-GGA functionals [90–92]. An accurate experimental value of the vacancy formation energy in Al is important for testing various numerical approaches for the description of surface energy corrections.

Table 2 shows that E_F = 0.63 eV calculated in the present work agrees well with the most recent *ab-initio* calculations reported in Refs. [41,54] performed using the PAW method together with the GGA approach for the exchange-correlation functional. The E_F values calculated within LDA are usually higher [81,84] indicating that the vacancy formation energy calculated using the LDA approach is slightly overestimated. Note that calculations in Refs. [82,84] were performed for constant supercell volume (only ion positions were relaxed). Neglecting of volume relaxation may lead to slightly different E_F values.

Note that our experimental and theoretical value are - with their respective errors - in excellent agreement with existing experiments cited in Ullmaier [76] and recent numerical results. Our experimental value of (0.62 ± 0.01) eV is compatible with the most probable value (0.67 ± 0.03) eV predicted in Ref. [76] within a little bit more than one σ.

3.3. Hydrogen-vacancy interaction

3.3.1. Positron lifetime spectroscopy

The positron lifetime results for the H-treated Al sample are shown in Fig. 10. Positron lifetime spectra can be well described by two components: a short-lived component with lifetime τ_1 representing a contribution of free positrons and a longer component with lifetime τ_2 which comes from positrons trapped at defects. At $T \leq 100$ K the H-treated sample shows a defect-related lifetime τ_2 = (228 ± 1) ps, which is 9 ps shorter than the value calculated for an isolated monovacancy in Al (237 ps), see Table 1, and also smaller than the experimental value for thermal equilibrium monovacancies, 240 ps (Fig. 6). The defect-related lifetime τ_2 = 228 ps measured in the H-treated sample is very close to the positron lifetime calculated for a vacancy associated with a single H atom (225 ps), see Table 1. This indicates that the sample annealed at 893 K in Varigon gas and then quenched contains most likely monovacancies associated with a single H atom (V-H complexes). Our *ab-initio* calculations show that trapping of up to 8 H atoms in a monovacancy is energetically favorable. Fig. 4 shows that H atoms trapped in a vacancy lead to a gradual shortening of the calculated positron lifetime from 237 ps for an isolated vacancy down to 190 ps for a vacancy associated with 8 H atoms. In the H-treated sample measured in the present work vacancies are associated only with single H atoms because the hydrogen concentration in the sample is rather low. The hydrogen solubility in the Al matrix is even at 893 K extremely low (< 0.01 at%) [93]. Hence, during annealing in Varigon gas atmosphere hydrogen is continuously entering and leaving the Al sample according to its thermodynamic equilibrium concentration. So the average hydrogen concentration in the sample remains at the low value given above. Because of the elevated annealing temperature (893 K) while diffusing hydrogen is continuously trapped and detrapped from vacancies. Similarly, during their diffusive motion vacancies are simultaneously created at sources and annealed at sinks inside the sample. Hence, a dynamic equilibrium between creation and disappearance of vacancies and between trapping and detrapping of hydrogen atoms is established. When the sample is then quenched to a temperature of 0 °C vacancies are “frozen” in the sample, while hydrogen in the matrix remains mobile and either leaves the sample by diffusion or finds a vacancy and becomes trapped there. As a consequence, one finds on average one hydrogen atom per vacancy.

Linderoth et al. [19] have studied proton-irradiated Al and found a defect-related positron lifetime of (240 ± 15) ps which the authors assigned to monovacancies with trapped H atoms. This lifetime agrees within its uncertainty with the lifetime of (240 ± 2) ps determined in the present work for bare vacancies but also with the lifetime of (228 ± 1) ps measured in the present work for the V-H complex. Note that the relatively small difference between the lifetime of positrons trapped in bare vacancies and in V-H complexes indicates the utmost importance of a precise measurement of positron lifetime with low uncertainty.

With increasing measurement temperature from 80 to 220 K, τ_2 in

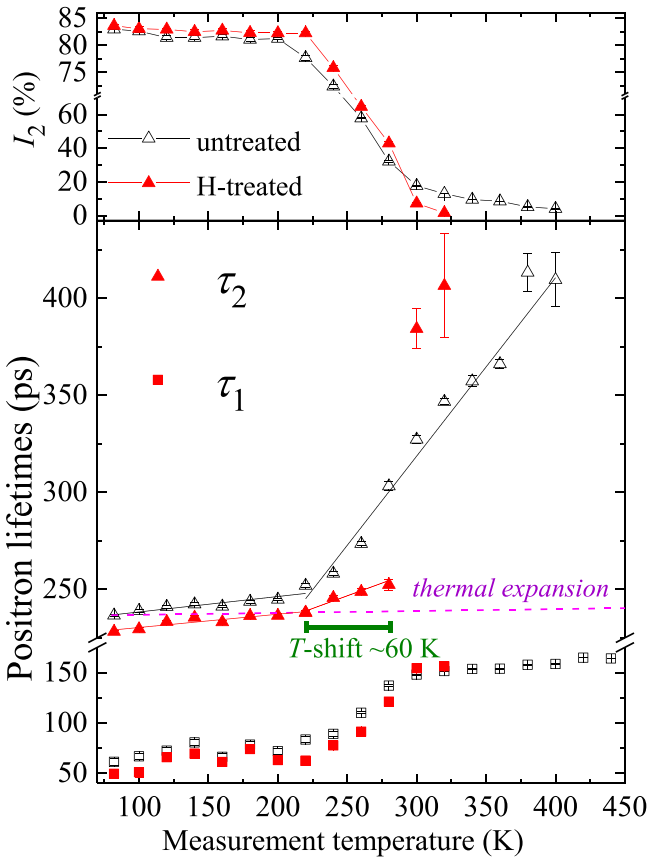

Fig. 10. Results of positron lifetime spectra decomposition of high-purity Al after 2 h heat treatment at 893 K under Varigon gas flow (H-treated) and then rapidly quenched to ice water (closed red symbols). The as-quenched samples were immediately moved to a LN_2 cryostat and measured in the temperature range ~ 80–440 K. Results for another sample subjected to the identical thermal treatment without Varigon (untreated) are shown for comparison (open symbols). The defect-related positron lifetime τ_2 (triangles) and the reduced bulk lifetime τ_1 (squares) are shown in the lower panel, while the intensity I_2 (diamonds) related to the τ_2 component is displayed in the upper panel. The straight solid lines are linear fits. The pink dashed line indicates the calculated increase of τ_2 caused by thermal lattice expansion. Trapped hydrogen shifts the mobility of vacancies from 220 to 280 K, i.e. to 60 K higher temperatures. This is referred to as temperature shift (T-shift). Note that the error bars are small (within the symbols for most data points) due to the high statistics. At high temperatures the uncertainties becomes larger owing to the distinct decrease of the intensity I_2. (For interpretation of the references to colour in this figure legend, the reader is referred to the web version of this article.)

the H-treated sample slowly increases by about 10 ps. Then it increases more rapidly in the range 220–280 K while remaining below 250 ps up to 280 K, and finally abruptly increases at higher temperatures. The slow approximately linear increase of τ_2 in the temperature range from 80 to 220 K exceeds the increase caused by thermal expansion of lattice (see dashed line in Fig. 10) and indicates that V-H complexes located close to each other likely merge into divacancies associated with hydrogen (2V-2H). Hence, in the temperature range 80–220 K the sample contains a mixture of vacancies and divacancies associated with hydrogen while the fraction of divacancies slowly increases with temperature. At $T =$ 240 K the lifetime τ_2 is close to the value of 244 ps calculated for positrons trapped in a divacancy associated with two H atoms (2V-2H complex) – probably formed by the agglomeration of two V-H complexes. Hence, at 240 K the sample contains mostly 2V-2H complexes. The steeper increase of τ_2 with temperature starting at 240 K indicates that 2V-2H complexes further agglomerate into larger defects. Nevertheless, in this stage vacancies occurring in the temperature range 240 – 280 K are still associated with hydrogen. By annealing above 280 K hydrogen is released from vacancies. As a consequence, the mobility of vacancies is increased and they either disappear by diffusion to sinks at grain boundaries or agglomerate into vacancy clusters. This is reflected by an abrupt increase of τ_2, which reached ≈ 385 and 405 ps at 300 and 320 K, respectively. From comparison of τ_2 with *ab-initio* calculations of lifetimes of positrons trapped in vacancy clusters of various sizes in Al [94] one can estimate that the vacancy clusters formed at 300 K consist on average of about 10 vacancies. By annealing to 320 K their average size increased to ≈ 16 vacancies. The intensity I_2 distinctly decreases above 220 K and vanishes at 350 K testifying that vacancy clusters were annealed out at this temperature.

The lifetime τ_1 of the free positron component is significantly lower than the bulk positron lifetime in Al (τ_b = 158 ps) due to positron trapping at defects in accordance with the simple trapping model [95]. A decreasing concentration of vacancies leads to an increase of τ_1 in particular in the temperature range 250–300 K, where mobile vacancies gradually disappear by diffusion to sinks at grain boundaries or on the surface. At temperatures above 300 K, when the concentration of defects becomes negligible, the lifetime τ_1 approaches the bulk positron lifetime for Al.

For comparison, an identical Al sample was treated similarly except of hydrogen loading, i.e. it was annealed at 893 K, quenched and measured in the temperature range ~ 80–440 K. One can see in Fig. 10 that the defect-related positron lifetime value τ_2 = (237 ± 2) ps is comparable to the calculated lifetime of positrons trapped in monovacancy in Al (Table 1) and very close to the value measured for thermal equilibrium monovacancies (240 ± 2 ps). Similar to the H-treated sample the lifetime τ_2 exhibits an approximately linear increase in the temperature range 80–220 K indicating that vacancies merge into divacancies. The lifetime τ_2 of positrons trapped in vacacny-defects remains below 250 ps up to 220 K. At higher temperatures τ_2 increases distinctly reaching a value of about 400 ps at 380 K, testifying that vacancies aggregate forming clusters consisting of about 16 vacancies. This agrees very well with previous studies, which reported that vacancies are mobile at about 220 K [19,69,96] and monovacancies freely migrate around 240 K [19,69,96] subsequently forming vacancy clusters. The intensity I_2 is found to be high at low temperatures and decreases distinctly at $T >$ 200 K and, finally, drops to a few % at 400 K indicating a decreasing concentration of vacancies. It is reported that vacancy clusters in Al anneal out between 400 and 530 K [97] and the released vacancies can annihilate at sinks such as grain boundaries or on the surface [19].

The lifetime of positrons trapped in vacancies (237 ps) measured in the untreated sample is very similar to that (τ_2 = 235 ps) obtained in pure Al quenched from 690 K into water by Calloni et al. [98]. However, the intensity I_2 = 58% reported by Calloni et al. [98] is significantly smaller than the value (I_2 = 84%) obtained in the present study. This is due to lower annealing temperature used in Ref. [98]. The equilibrium concentration of vacancies exponentially increases with temperature according to Eq. (13). Using the vacancy formation entropy $S_F = 1.03\ k_B$ and the vacancy formation energy E_F = 0.62 eV Eq. (13) yields an equilibrium concentration of vacancies of 8.3×10^{-5} and 8.9×10^{-4} at.$^{-1}$ at 690 and 893 K, respectively. Hence, the equilibrium concentration of vacancies at 893 K is ≈ 11 times higher than at 690 K. Higher concentration of vacancies results in higher intensity I_2 for the sample quenched from 893 K.

Our experiment showed that hydrogen is trapped at vacancies up to 280 K. This is in accordance with the data reported by Linderoth et al. [19], who found that hydrogen stabilizes monovacancies in Al up to 295 K. A significantly smaller slope of the increase of τ_2 with temperature in the range 240–280 K compared to the untreated sample testifies that trapped hydrogen decreases the mobility of vacancies. This is related to the observation that an abrupt increase of τ_2 caused by the agglomeration of vacancies into clusters is shifted to about of 60 K higher temperature in the H-treated sample, see Fig. 10. Note that hydrogen

trapping in vacancies lowers the H diffusivity in the Al matrix [99] and may reduce the aluminum ductility, which is consistent with previous studies [100–102].

In addition, slightly higher intensity I_2 in the H-loaded sample, compared to its corresponding value in the untreated sample in the temperature range 80–200 K indicates an enhancement of vacancy formation and, thus, a lowering of its formation energy. This implies that hydrogen assists the formation of vacancies in Al as predicted theoretically [4] and lowers the vacancy formation energy like in other metals [103].

A comparison of the average positron lifetime τ_{av} for the H-treated and untreated sample is plotted in Fig. 11. For the H-treated Al sample τ_{av} is about 200 ps at low temperatures and increases very slightly ($\sim$ 5 ps) in the temperature range up to 250 K thanks to a slight increase of τ_2 since its intensity I_2 is dominating. A decrease of τ_{av} at $T > 250$ K is due to a loss of freely migrating vacancies when hydrogen bound to vacancies is released.

The concentration of defects can be calculated from PALS data in Figs. 10 and 11 using the two state simple trapping model [95] as

$$C = \frac{1}{\mu}\frac{1}{\tau_b}\frac{\tau_{av}-\tau_b}{\tau_2-\tau_{av}} \tag{15}$$

where μ is the positron trapping coefficient for the kind of defects present in the sample. The positron trapping coefficient for monovacancies in Al is $\mu_{1v} = 2.5 \times 10^{14}$ s^{-1} [69,78]. For small vacancy clusters the trapping coefficient is directly proportional to the number of vacancies n the cluster consists of, i.e. $\mu \approx n\,\mu_{1v}$ [104]. The average number of vacancies n was obtained from comparison of the lifetime τ_2 with the results of *ab-initio* calculations in the present paper and in Ref. [94]. Fig. 12(a) shows the concentration of defects C calculated using Eq. (15) for H-treated and untreated samples. Obviously, C continuously decreases with annealing temperature because coalescence of small defects into larger ones decreases the overall concentration of defects, i.e. the number of defects per host atom. Since vacancy clusters consist on average of n vacancies the net concentration of vacancies in the sample, C_v, was calculated from the concentration of defects, C, as $C_v = n\,C$ and is plotted in Fig. 12(b). From inspection of the figure one can conclude that at low temperatures $T < 220$ K, where vacancies start to merge into divacancies, the total concentration of vacancies C_v in the sample remains approximately constant, i.e. vacancies only coalesce but their total number remains unchanged. In contrast, at higher temperatures, where vacancy clusters are formed, C_v decreases because vacancies become more mobile and some of them disappear by diffusion to sinks at grain boundaries and on the surface and, thus, only a fraction of vacancies is incorporated in vacancy clusters. Hence, the total number of vacancies gradually decreases. Moreover, one can see from Fig. 12(b) that the H-treated sample contains a slightly higher concentration of quenched-in vacancies than the untreated one suggesting that absorbed hydrogen lowers the vacancy formation energy in accordance with the theoretical prediction [93]. Note that the concentration of vacancies measured in the quenched sample is one order of magnitude lower than the estimated concentration of equilibrium vacancies at the annealing temperature of 893 K. Thus, about 90% of thermal vacancies disappeared during quenching.

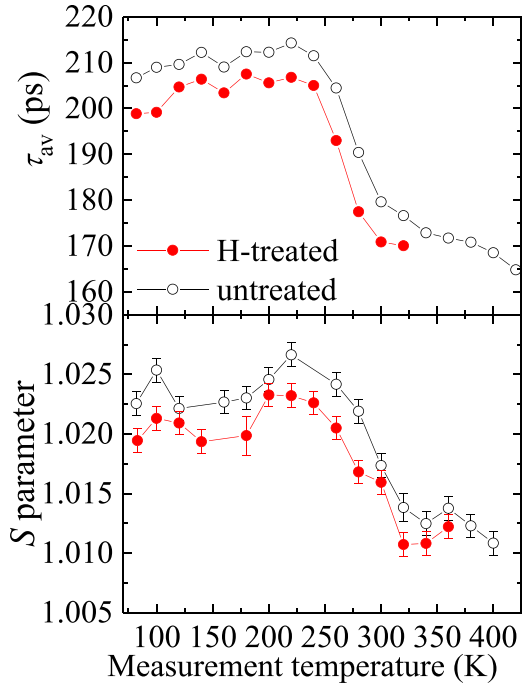

Fig. 11. The S parameter (lower panel) and the average positron lifetime (upper panel) calculated from the lifetime spectra decomposition in Fig. 9 as a function of the measurement temperature for the H-treated Al (red solid circles) and H-untreated Al sample (black open circles). High purity Al was annealed 2 h at 893 K and then rapidly quenched into ice water. Each point in the figure corresponds to keeping the sample at the corresponding temperature during the measurement: 2 h for PALS and 0.5 h for DBS. (For interpretation of the references to colour in this figure legend, the reader is referred to the web version of this article.)

It has to be mentioned that the microstructure of Al samples may gradually change during 2 h period of PALS measurement at temperatures where vacancies are mobile, i.e. above 220 and 280 K for H-treated and untreated sample, respectively. To estimate the extent of these changes kinetic PALS measurements of a quenched sample at ambient temperature (300 K), i.e. at a temperature where vacancies are mobile both in the H-treated and untreated sample, were performed and are described in detail in the supplementary material (section S3). These kinetic measurements confirmed that changes of the microstructure during 2 h of PALS measurement period are rather small compared to changes caused by the increasing temperature.

3.3.2. *Doppler broadening spectroscopy*

The lower panel in Fig. 11 shows a comparison of the S parameter measured in H-treated and untreated Al. The temperature dependence of the S parameter is very similar to the behavior of the average positron lifetime. The presence of an H atom trapped in a monovacancy increases the local electron density, which is reflected by a decrease of the S parameter.

For the H-charged sample, the S parameter starts to decrease at $T >$ 250 K owing to the dissociation of V-H complexes. Released vacancies are mobile above 220 K and, thus, agglomerate forming vacancy clusters. The sample treated without hydrogen shows a higher S parameter than the H-treated one since the electron density in bare vacancies is lower than in V-H complexes. In addition, a decrease of the S parameter starts at lower temperature in the samples not loaded with hydrogen.

4. Conclusions

Positron lifetime, conventional Doppler, and coincidence Doppler broadening spectroscopies were employed to study thermal vacancies and their interaction with hydrogen in high-purity Al. *Ab-initio* calculations of vacancy-nH complexes were performed in the relaxed geometry and gave results in very good agreement with our experimental results.

Thermal equilibrium monovacancies were detected by all PAS techniques. The vacancy formation energy determined from PAS data is (0.62±0.01) eV in excellent agreement with our *ab-initio* calculations (0.63 eV), reducing thereby the uncertainty for the vacancy formation energy as well as the discrepancy between experiment and theory. The vacancy formation entropy $S_F = (1.03 \pm 0.01)\,k_B$ was determined from PAS data as well.

The high-purity Al has been loaded with hydrogen during thermal

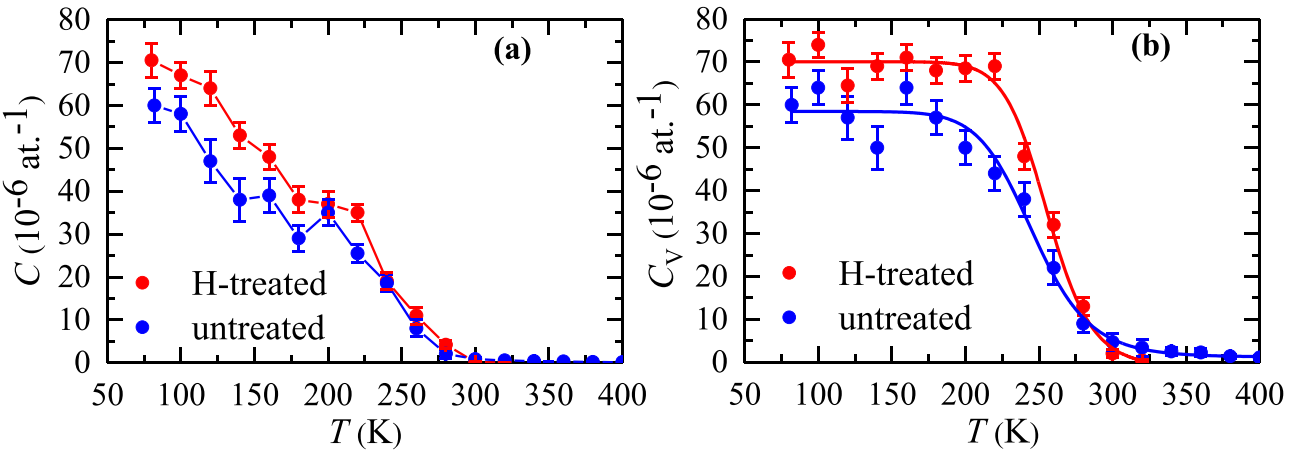

Fig. 12. Temperature dependence of (a) the concentration of defects C; (b) the net concentration of vacancies C_V calculated from PALS data in Figs. 10 and 11.

annealing at 893 K in Varigon gas followed by rapid quenching to ice water. Single H atoms trapped at monovacancies were observed. The experimental positron lifetime of 228 ± 1 ps of this defect is very close to the value of 225 ps calculated for the V-H complex. With increasing temperature V-H complexes gradually merge into 2V-2H complexes due to the higher stability of the latter. Hydrogen is found to stabilize vacancies up to about 280 K. This shifts the onset of vacancy migration from 220 K for the untreated sample to 280 K for the H-treated sample. At 280 K hydrogen is released from vacancies and now freely migrating vacancies quickly agglomerate into vacancy clusters or disappear by diffusion to sinks at grain boundaries and on the surface.

Our experiments showed that both PALS and DBS methods are sensitive to hydrogen trapping in vacancies, where both positron parameters (lifetime and S) are found to be lower than their corresponding values for pure vacancies. Although *ab-initio* calculations showed that a mono-vacancy is capable of trapping multiple H atoms, exclusively vacancies associated with single H atoms were detected in our work, where Al samples have been H-treated in Varigon gas. This can be attributed to the low hydrogen concentration introduced into our samples.

Declaration of Competing Interest

The authors declare that they have no known competing financial interests or personal relationships that could have appeared to influence the work reported in this paper.

Acknowledgments

Computational resources for *ab-initio* calculations were supplied by the e-INFRA CZ project (ID:90140), supported by the Ministry of Education, Youth and Sports of the Czech Republic. We would like to thank M.O. Liedke (Helmholtz-Zentrum Dresden-Rossendorf, Dresden) for providing the slow positron beam measurements and for the fruitful discussion.

Supplementary materials

Supplementary material associated with this article can be found, in the online version, at doi:10.1016/j.actamat.2023.118770.

References

[1] G. Alefeld, J. Völkl, Hydrogen in metals. Topics Applied Physics, Springer, Berlin, 1978.
[2] F. Besenbacher, S.M. Myers, J.K. NØrskov, Interaction of hydrogen with defects in metals, Nucl. Instrum. Methods Phys. Res. B7/8 (1985) 55–66.
[3] M.A. Quiroga, C. Macchi, A. Somoza, Vacancy assisted solute transport mechanisms responsible for the solute atom agglomeration during the early stages of aging in Al-Cu-based alloys, Phys. Rev. Mater. 6 (2022) 33603, https://doi.org/10.1103/PhysRevMaterials.6.033603.
[4] G. Lu, E. Kaxiras, Hydrogen embrittlement of aluminum: the crucial role of vacancies, Phys. Rev. Lett. 94 (2005), 155501, https://doi.org/10.1103/PhysRevLett.94.155501.
[5] G. Ho, M.T. Ong, K.J. Caspersen, E.A. Carter, Energetics and kinetics of vacancy diffusion and aggregation in shocked aluminium via orbital-free density functional theory, Phys. Chem. Chem. Phys. 9 (2007) 4951–4966, https://doi.org/10.1039/B705455F.
[6] M.J. Couper, A.E. Neeson, J.R. Griffiths, Casting defects and the fatigue behaviour of an aluminium casting alloy, Fatigue Fract. Eng. Mater. Struct. 13 (1990) 213–227, https://doi.org/10.1111/j.1460-2695.1990.tb00594.x.
[7] P.N. Anyalebechi, Hydrogen diffusion in Al-Li alloys, Metall. Trans. B 21 (1990) 649–655, https://doi.org/10.1007/BF02654243.
[8] C.H. Zamponi, S.T. Sonneberger, M. Haaks, I. Müller, T. Staab, G. Tempus, K. Maier, Investigation of fatigue cracks in aluminium alloys 2024 and 6013 in laboratory air and corrosive environment, J. Mater. Sci. 39 (2004) 6951–6956, https://doi.org/10.1023/B:JMSC.0000047537.16498.1d.
[9] C. Wolverton, V. Ozoliņš, M. Asta, Hydrogen in aluminum: first-principles calculations of structure and thermodynamics, Phys. Rev. B 69 (2004), 144109, https://doi.org/10.1103/PhysRevB.69.144109.
[10] W.A. Counts, C. Wolverton, R. Gibala, First-principles energetics of hydrogen traps in α-Fe: point defects, Acta Mater. 58 (2010) 4730–4741, https://doi.org/10.1016/j.actamat.2010.05.010.
[11] W. Xing, X.Q. Chen, Q. Xie, G. Lu, D. Li, Y. Li, Unified mechanism for hydrogen trapping at metal vacancies, Int. J. Hydrog. Energy 39 (2014) 11321–11327, https://doi.org/10.1016/j.ijhydene.2014.05.032.
[12] Z.D. Popovic, M.J. Stott, Nonlinear, self-consistent theory of proton screening in metals applied to hydrogen in Al and Mg, Phys. Rev. Lett. 33 (1974) 1164–1167, https://doi.org/10.1103/PhysRevLett.33.1164.
[13] P. Jena, M.J. Ponnambalam, Positron annihilation as a probe for impurities trapped by vacancy clusters, Phys. Rev. B 26 (1982) 5264–5267, https://doi.org/10.1103/PhysRevB.26.5264.
[14] K. Iyakutti, J.L. Calais, Electronic structure of vacancies and hydrogen-trapped vacancies in aluminium with application to the positron lifetime calculation, J. Phys. F Met. Phys. 13 (1983) 1–11, https://doi.org/10.1088/0305-4608/13/1/003.
[15] H.E. Hansen, R.M. Nieminen, M.J. Puska, Computational analysis of positron experiments, J. Phys. F Met. Phys. 14 (1984) 1299–1316, https://doi.org/10.1088/0305-4608/14/5/025.
[16] M.J. Puska, R.M. Nieminen, Defect spectroscopy with positrons: a general calculational method, J. Phys. F Met. Phys. 13 (1983) 333–346, https://doi.org/10.1088/0305-4608/13/2/009.
[17] H. Gunaydin, S.V. Barabash, K.N. Houk, V. Ozoliņš, First-principles theory of hydrogen diffusion in aluminum, Phys. Rev. Lett. 101 (2008), 075901, https://doi.org/10.1103/PhysRevLett.101.075901.
[18] Y. Fukai, Superabundant vacancies formed in metalhydrogen alloys, Phys. Scr. T103 (2003) 11, https://doi.org/10.1238/physica.topical.103a00011.
[19] S. Linderoth, H. Rajainmäki, R.M. Nieminen, Defect recovery in aluminum irradiated with protons at 20K, Phys. Rev. B 35 (1987) 5524–5528, https://doi.org/10.1103/PhysRevB.35.5524.
[20] Y. Fukai, N. Ōkuma, Formation of superabundant vacancies in Pd hydride under high hydrogen pressures, Phys. Rev. Lett. 73 (1994) 1640–1643, https://doi.org/10.1103/PhysRevLett.73.1640.
[21] Y. Fukai, Formation of superabundant vacancies in M–H alloys and some of its consequences: a review, J. Alloy. Compd. 356–357 (2003) 263–269, https://doi.org/10.1016/S0925-8388(02)01269-0.
[22] A. Pundt, R. Kirchheim, Hydrogen in metals: microstructural aspects, Annu. Rev. Mater. Res. 36 (2006) 555–608, https://doi.org/10.1146/annurev.matsci.36.090804.094451.

[23] G. Hachet, X. Sauvage, Hydrogen delaying the formation of Guinier-Preston zones in aluminium alloys, Acta Mater. (2022), 118373, https://doi.org/10.1016/j.actamat.2022.118373.

[24] P. Hautojärvi, A. Dupasquier, M.J. Manninen, P.E. Mijnarends, R.M. Nieminen, A. Vehanen, R.N. West, Positrons in Solids: Topics in Current Physics, Springer, Berlin, Heidelberg, 1979, https://doi.org/10.1007/978-3-642-81316-0.

[25] W. Brandt, A. Dupasquier, W. Brandt, A. Dupasquier, Positron Solid-State Physics, in: Proceedings of the International Scheme Physics "Enrico Fermi", North-Holland, Amsterdam, 1983.

[26] P. Hautojärvi, C. Corbel, A. Dupasquier, A.P. Mills, Positron spectroscopy of solids, in: Proceedings of the International Scheme Physics "Enrico Fermi", Amsterdam, IOS Press, 1995.

[27] M. Eldrup, A.V Chadwick, M. Terenzi, Application of the positron annihilation technique in studies of defects in solids. Defects in Solids, Springer US, Plenum Press, New York, 1986, pp. 145–178, https://doi.org/10.1007/978-1-4757-0761-8_7.

[28] M. Elsayed, A.M. Ibrahim, T.E.M. Staab, R. Krause-Rehberg, A new perspective on the precipitation sequence in a high-purity Al-1.74at.%Cu alloy by employing positron annihilation spectroscopy: experiment and theory, J. Phys. Condens. Matter 33 (2021), 435401. http://iopscience.iop.org/article/10.1088/1361-648X/ac17af.

[29] M. Elsayed, T.E.M. Staab, J. Čížek, R. Krause-Rehberg, On the interaction of solute atoms with vacancies in diluted Al-alloys: a paradigmatic experimental and ab-initio study on indium and tin, Acta Mater. 219 (2021), 117228, https://doi.org/10.1016/j.actamat.2021.117228.

[30] S.T. Picraux, Defect trapping of gas atoms in metals, Nucl. Instrum. Methods (1981) 413–437.

[31] T. Ishikawa, R.B. McLellan, The diffusivity of hydrogen in aluminum, Acta Metall. 34 (1986) 1091–1095, https://doi.org/10.1016/0001-6160(86)90219-1.

[32] S. Lynch, Hydrogen embrittlement phenomena and mechanisms, 30 (2012) 105–123. 10.1515/corrrev-2012-0502.

[33] F. Lotter, U. Muehle, M. Elsayed, A.M. Ibrahim, T. Schubert, R. Krause-Rehberg, B. Kieback, T.E.M. Staab, Precipitation behavior in high-purity aluminium alloys with trace elements – the role of quenched-in vacancies, Phys. Status Solidi Appl. Mater. Sci. 215 (2018) 1–11, https://doi.org/10.1002/pssa.201800375.

[34] M. Elsayed, R. Krause-Rehberg, C. Eisenschmidt, N. Eißmann, B. Kieback, Defect study in CoCrFeMnNi high entropy alloy by positron annihilation lifetime spectroscopy, Phys. Status Solidi Appl. Mater. Sci. 215 (2018), https://doi.org/10.1002/pssa.201800036.

[35] J. Kansy, Microcomputer program for analysis of positron annihilation lifetime spectra, Nucl. Instrum. Methods Phys. Res. A 374 (1996) 235–244, https://doi.org/10.1016/0168-9002(96)00075-7.

[36] J. Čížek, M. Vlček, I. Procházka, Digital spectrometer for coincidence measurement of Doppler broadening of positron annihilation radiation, Nucl. Instrum. Methods Phys. Res. Sect. A Accel. Spectrom. Detect. Assoc. Equip. 623 (2010) 982–994.

[37] J. Čížek, M. Vlček, I. Procházka, Investigation of positron annihilation-in-flight using a digital coincidence Doppler broadening spectrometer, New J. Phys. 14 (2012) 35005, https://doi.org/10.1088/1367-2630/14/3/035005.

[38] G. Kresse, J. Hafner, *Ab initio* molecular dynamics for liquid metals, Phys. Rev. B 47 (1993) 558–561, https://doi.org/10.1103/PhysRevB.47.558.

[39] G. Kresse, J. Furthmüller, Efficient iterative schemes for ab initio total-energy calculations using a plane-wave basis set, Phys. Rev. B 54 (1996) 11169–11186, https://doi.org/10.1103/PhysRevB.54.11169.

[40] H.J. Monkhorst, J.D. Pack, Special points for Brillouin-zone integrations, Phys. Rev. B 13 (1976) 5188–5192, https://doi.org/10.1103/PhysRevB.13.5188.

[41] C. Freysoldt, B. Grabowski, T. Hickel, J. Neugebauer, G. Kresse, A. Janotti, C. G. Van de Walle, First-principles calculations for point defects in solids, Rev. Mod. Phys. 86 (2014) 253–305, https://doi.org/10.1103/RevModPhys.86.253.

[42] K. Heinola, T. Ahlgren, K. Nordlund, J. Keinonen, Hydrogen interaction with point defects in tungsten, Phys. Rev. B 82 (2010) 94102, https://doi.org/10.1103/PhysRevB.82.094102.

[43] Y. Tateyama, T. Ohno, Stability and clusterization of hydrogen-vacancy complexes in α-Fe: an *ab initio* study, Phys. Rev. B 67 (2003), 174105, https://doi.org/10.1103/PhysRevB.67.174105.

[44] A. San-Martin, F.D. Manchester, The Al-H (aluminum-hydrogen) system, J. Phase Equilibr. 13 (1992) 17–21, https://doi.org/10.1007/BF02645371.

[45] M.J. Puska, R.M. Nieminen, Theory of positrons in solids and on solid surfaces, Rev. Mod. Phys. 66 (1994) 841–897, https://doi.org/10.1103/RevModPhys.66.841.

[46] E. Boroński, R.M. Nieminen, Electron-positron density-functional theory, Phys. Rev. B 34 (1986) 3820–3831, https://doi.org/10.1103/PhysRevB.34.3820.

[47] T. Korhonen, M.J. Puska, R.M. Nieminen, First-principles calculation of positron annihilation characteristics at metal vacancies, Phys. Rev. B 54 (1996) 15016–15024, https://doi.org/10.1103/PhysRevB.54.15016.

[48] J. Wiktor, G. Jomard, M. Torrent, Two-component density functional theory within the projector augmented-wave approach: accurate and self-consistent computations of positron lifetimes and momentum distributions, Phys. Rev. B 92 (2015), 125113, https://doi.org/10.1103/PhysRevB.92.125113.

[49] X. Gonze, B. Amadon, G. Antonius, F. Arnardi, L. Baguet, J.M. Beuken, J. Bieder, F. Bottin, J. Bouchet, E. Bousquet, N. Brouwer, F. Bruneval, G. Brunin, T. Cavignac, J.B. Charraud, W. Chen, M. Côté, S. Cottenier, J. Denier, G. Geneste, P. Ghosez, M. Giantomassi, Y. Gillet, O. Gingras, D.R. Hamann, G. Hautier, X. He, N. Helbig, N. Holzwarth, Y. Jia, F. Jollet, W. Lafargue-Dit-Hauret, K. Lejaeghere, M.A.L. Marques, A. Martin, C. Martins, H.P.C. Miranda, F. Naccarato, K. Persson, G. Petretto, V. Planes, Y. Pouillon, S. Prokhorenko, F. Ricci, G.-.M. Rignanese, A. H. Romero, M.M. Schmitt, M. Torrent, M.J. van Setten, B. Van Troeye, M. J. Verstraete, G. Zérah, J.W. Zwanziger, The Abinitproject: impact, environment and recent developments, Comput. Phys. Commun. 248 (2020), 107042, https://doi.org/10.1016/j.cpc.2019.107042.

[50] I. Makkonen, M. Hakala, M.J. Puska, Modeling the momentum distributions of annihilating electron-positron pairs in solids, Phys. Rev. B 73 (2006) 35103, https://doi.org/10.1103/PhysRevB.73.035103.

[51] M. Alatalo, B. Barbiellini, M. Hakala, H. Kauppinen, T. Korhonen, M.J. Puska, K. Saarinen, P. Hautojärvi, R.M. Nieminen, Theoretical and experimental study of positron annihilation with core electrons in solids, Phys. Rev. B 54 (1996) 2397–2409, https://doi.org/10.1103/PhysRevB.54.2397.

[52] B. Barbiellini, M.J. Puska, T. Korhonen, A. Harju, T. Torsti, R.M. Nieminen, Calculation of positron states and annihilation in solids: a density-gradient-correction scheme, Phys. Rev. B 53 (1996) 16201–16213, https://doi.org/10.1103/PhysRevB.53.16201.

[53] N.A.W. Holzwarth, A.R. Tackett, G.E. Matthews, A projector augmented wave (PAW) code for electronic structure calculations, Part I: atompaw for generating atom-centered functions, Comput. Phys. Commun. 135 (2001) 329–347, https://doi.org/10.1016/S0010-4655(00)00244-7.

[54] I. Kohlbach, B. Korff, T.E.M. Staab, (Meta-)stable phases and pre-Guinier-Preston zones in AlCu alloys constructed from ab initio relaxed atomic positions - comparison to experimental methods, Phys. Status Solidi Basic Res. 247 (2010) 2168–2178, https://doi.org/10.1002/pssb.201046102.

[55] J.P. Bugeat, A.C. Chami, E. Ligeon, A study of hydrogen implanted in aluminium, Phys. Lett. A 58 (1976) 127–130, https://doi.org/10.1016/0375-9601(76)90520-X.

[56] R. Nazarov, T. Hickel, J. Neugebauer, *Ab initio* study of H-vacancy interactions in fcc metals: implications for the formation of superabundant vacancies, Phys. Rev. B 89 (2014), 144108, https://doi.org/10.1103/PhysRevB.89.144108.

[57] Z.D. Popovic, M.J. Stott, J.P. Carbotte, G.R. Piercy, Theory of the heat of solution of hydrogen in Al and Mg using nonlinear screening, Phys. Rev. B 13 (1976) 590–602, https://doi.org/10.1103/PhysRevB.13.590.

[58] R.A.H. Edwards, W. Eichenauer, Reversible hydrogen trapping at grain boundaries in superpure aluminium, Scr. Metall. 14 (1980) 971–973.

[59] M. Ichimura, H. Katsuta, Y. Sasajima, M. Imabayashi, Hydrogen and deuterium solubility in aluminum with voids, J. Phys. Chem. Solids 49 (1988) 1259–1267, https://doi.org/10.1016/0022-3697(88)90184-9.

[60] H. Sugimoto, Y. Fukai, Solubility of hydrogen in metals under high hydrogen pressures: thermodynamical calculations, Acta Metall. Mater. 40 (1992) 2327–2336, https://doi.org/10.1016/0956-7151(92)90151-4.

[61] F.D. Manchester, Phase Diagrams of Binary Hydrogen Alloys, ASM International, Materials Park OH, 2000.

[62] D.S. Larsen, J.K. NØrskov, Calculated energies and geometries for hydrogen impurities in Al and Mg, J. Phys. F Met. Phys. 9 (1979) 1975.

[63] S.M. Myers, F. Besenbacher, J.K. NØrskov, Immobilization mechanisms for ion-implanted deuterium in aluminum, J. Appl. Phys. 58 (1985) 1841–1850, https://doi.org/10.1063/1.336037.

[64] T.M. Hall, A.N. Goland, C.L. Snead, Applications of positron-lifetime measurements to the study of defects in metals, Phys. Rev. B 10 (1974) 3062–3074, https://doi.org/10.1103/PhysRevB.10.3062.

[65] M. Liu, J. Čížek, C.S.T. Chang, J. Banhart, Early stages of solute clustering in an Al-Mg-Si alloy, Acta Mater. 91 (2015) 355–364, https://doi.org/10.1016/j.actamat.2015.02.019.

[66] H.E. Schaefer, R. Gugelmeier, M. Schmolz, A. Seeger, Positron lifetime spectroscopy and trapping at vacancies in aluminium, Mater. Sci. Forum 15-18 (1987) 111–116, https://doi.org/10.4028/www.scientific.net/MSF.15-18.111.

[67] T.E.M. Staab, E. Zschech, R. Krause-Rehberg, Positron lifetime measurements for characterization of nano-structural changes in the age hardenable AlCuMg 2024 alloy, J. Mater. Sci. 35 (2000) 4667–4672, https://doi.org/10.1023/A:1004838619943.

[68] K.G. Lynn, J.E. Dickman, W.L. Brown, M.F. Robbins, E. Bonderup, Vacancies studied by positron annihilation with high-momentum core electrons, Phys. Rev. B 20 (1979) 3566–3572.

[69] J.A. Jackman, G.M. Hood, R.J. Schultz, Positron lifetime measurements of the vacancy properties of annealed and electron-irradiated aluminium, J. Phys. F Met. Phys. 17 (1987) 1817–1831, https://doi.org/10.1088/0305-4608/17/9/009.

[70] A.M. James, M.P. Lord, Macmillan's Chemical and Physical Data, Macmillan, London, UK, 1992.

[71] M.J. Fluss, L.C. Smedskjaer, M.K. Chason, D.G. Legnini, R.W. Siegel, Measurements of the vacancy formation enthalpy in aluminum using positron annihilation spectroscopy, Phys. Rev. B 17 (1978) 3444–3455, https://doi.org/10.1103/PhysRevB.17.3444.

[72] C. Hugenschmidt, Positrons in surface physics, Surf. Sci. Rep. 71 (2016) 547–594, https://doi.org/10.1016/j.surfrep.2016.09.002.

[73] C.L. Snead, T.M. Hall, A.N. Goland, Vacancy-impurity binding energy in aluminum-1.7 at.% zinc using positron-annihilation lifetimes, Phys. Rev. Lett. 29 (1972) 62–65, https://doi.org/10.1103/PhysRevLett.29.62.

[74] P. Tzanetakis, J. Hillairet, G. Revel, The formation energy of vacancies in aluminium and magnesium, Phys. Status Solidi 75 (1976) 433–439, https://doi.org/10.1002/pssb.2220750205.

[75] B. Bergersen, M.J. Stott, The effect of vacancy formation on the temperature dependence of the positron lifetime, Solid State Commun. 7 (1969) 1203–1205, https://doi.org/10.1016/0038-1098(69)90177-X.

[76] H. Ullmaier, Landolt-Börnstein, numerical data and functional relationships in science and technology, new series, group iii: crystal and solid state physics, vol.

25, atomic defects in metals. Berichte Der Bunsengesellschaft Für Phys. Chemie, Springer-Verlag, Berlin, 1991, https://doi.org/10.1002/bbpc.19930970923.
[77] K.G. Lynn, P.J. Schultz, Vacancy formation energy measurements in single crystal aluminum using a variable-energy positron beam, Appl. Phys. A 37 (1985) 31–36.
[78] E. Gramsch, K.G. Lynn, Trapping model for thermal and nonthermal positrons in metals, Phys. Rev. B 40 (1989) 2537–2540, https://doi.org/10.1103/PhysRevB.40.2537.
[79] T. Hehenkamp, Absolute vacancy concentrations in noble metals and some of their alloys, J. Phys. Chem. Solids 55 (1994) 907–915, https://doi.org/10.1016/0022-3697(94)90110-4.
[80] K.M. Carling, G. Wahnström, T.R. Mattsson, N. Sandberg, G. Grimvall, Vacancy concentration in Al from combined first-principles and model potential calculations, Phys. Rev. B 67 (2003) 54101, https://doi.org/10.1103/PhysRevB.67.054101.
[81] K. Carling, G. Wahnström, T.R. Mattsson, A.E. Mattsson, N. Sandberg, G. Grimvall, Vacancies in metals: from first-principles calculations to experimental data, Phys. Rev. Lett. 85 (2000) 3862–3865, https://doi.org/10.1103/PhysRevLett.85.3862.
[82] A. De Vita, M.J. Gillan, The ab initio calculation of defect energetics in aluminium, J. Phys. Condens. Matter. 3 (1991) 6225–6237, https://doi.org/10.1088/0953-8984/3/33/002.
[83] I.K. MacKenzie, P.C. Lichtenberger, Vacancy formation energies from positron trapping measurements, Appl. Phys. 9 (1976) 331–334, https://doi.org/10.1007/BF00900459.
[84] B. Medasani, M. Haranczyk, A. Canning, M. Asta, Vacancy formation energies in metals: a comparison of MetaGGA with LDA and GGA exchange–correlation functionals, Comput. Mater. Sci. 101 (2015) 96–107, https://doi.org/10.1016/j.commatsci.2015.01.018.
[85] A. Seeger, Investigation of point defects in equilibrium concentrations with particular reference to positron annihilation techniques, J. Phys. F Met. Phys. 3 (1973) 248–294, https://doi.org/10.1088/0305-4608/3/2/003.
[86] R. Nazarov, T. Hickel, J. Neugebauer, Vacancy formation energies in fcc metals: influence of exchange-correlation functionals and correction schemes, Phys. Rev. B 85 (2012), 144118, https://doi.org/10.1103/PhysRevB.85.144118.
[87] J.P. Perdew, A. Ruzsinszky, G.I. Csonka, O.A. Vydrov, G.E. Scuseria, L. A. Constantin, X. Zhou, K. Burke, Restoring the density-gradient expansion for exchange in solids and surfaces, Phys. Rev. Lett. 100 (2008), 136406, https://doi.org/10.1103/PhysRevLett.100.136406.
[88] L. Vitos, B. Johansson, J. Kollár, H.L. Skriver, Exchange energy in the local Airy gas approximation, Phys. Rev. B 62 (2000) 10046–10050, https://doi.org/10.1103/PhysRevB.62.10046.
[89] R. Armiento, A.E. Mattsson, Functional designed to include surface effects in self-consistent density functional theory, Phys. Rev. B 72 (2005), 085108, https://doi.org/10.1103/PhysRevB.72.085108.
[90] J.P. Perdew, A. Ruzsinszky, G.I. Csonka, L.A. Constantin, J. Sun, Workhorse semilocal density functional for condensed matter physics and quantum chemistry, Phys. Rev. Lett. 103 (2009), 026403, https://doi.org/10.1103/PhysRevLett.103.026403.
[91] J.P. Perdew, A. Ruzsinszky, G.I. Csonka, L.A. Constantin, J. Sun, Erratum: workhorse semilocal density functional for condensed matter physics and quantum chemistry [Phys. Rev. Lett. 103, 026403 (2009)], Phys. Rev. Lett. 106 (2011), 179902, https://doi.org/10.1103/PhysRevLett.106.179902.
[92] J. Sun, B. Xiao, Y. Fang, R. Haunschild, P. Hao, A. Ruzsinszky, G.I. Csonka, G. E. Scuseria, J.P. Perdew, Density functionals that recognize covalent, metallic, and weak bonds, Phys. Rev. Lett. 111 (2013), 106401, https://doi.org/10.1103/PhysRevLett.111.106401.
[93] C. Qiu, G.B. Olson, S.M. Opalka, D.L. Anton, Thermodynamic evaluation of the Al-H system, J. Ph. Equilibr. Diffus. 25 (2004) 520–527, https://doi.org/10.1007/s11669-004-0065-1.
[94] J. Čížek, M. Janeček, T. Vlasák, B. Smola, O. Melikhova, R.K. Islamgaliev, S. V. Dobatkin, The development of vacancies during severe plastic deformation, Mater. Trans. 60 (2019) 1533–1542, https://doi.org/10.2320/matertrans.MF201937.
[95] R.N. West, Positron studies of condensed matter, Adv. Phys. 22 (1973) 263–383, https://doi.org/10.1080/00018737300101299.
[96] R.W. Balluffi, Vacancy defect mobilities and binding energies obtained from annealing studies, J. Nucl. Mater. 69–70 (1978) 240–263, https://doi.org/10.1016/0022-3115(78)90247-7.
[97] J.E. Epperson, R.W. Hendricks, K. Farrell, Studies of voids in neutron-irradiated aluminium single crystals: I. Small-angle X-ray scattering and transmission electron microscopy, Philos. Mag. A J. Theor. Exp. Appl. Phys. 30 (1974) 803–817, https://doi.org/10.1080/14786437408207236.
[98] A. Calloni, A. Dupasquier, R. Ferragut, P. Folegati, M.M. Iglesias, I. Makkonen, M. J. Puska, Positron localization effects on the Doppler broadening of the annihilation line: aluminum as a case study, Phys. Rev. B 72 (2005) 54112, https://doi.org/10.1103/PhysRevB.72.054112.
[99] G.A. Young, J.R. Scully, The diffusion and trapping of hydrogen in high purity aluminum, Acta Mater. 46 (1998) 6337–6349, https://doi.org/10.1016/S1359-6454(98)00333-4.
[100] G. Zhang, G. Huang, M. Hu, F. Yang, L. Liu, J. Konys, T. Tang, Stability and clusterization of hydrogen-vacancy complexes in B2-FeAl: insight from hydrogen embrittlement, RSC Adv. 7 (2017) 11094–11100, https://doi.org/10.1039/C6RA27936H.
[101] H. Zhao, P. Chakraborty, D. Ponge, T. Hickel, B. Sun, C.H. Wu, B. Gault, D. Raabe, Hydrogen trapping and embrittlement in high-strength Al alloys, Nature 602 (2022) 437–441, https://doi.org/10.1038/s41586-021-04343-z.
[102] A.V. Bochkaryova, Y.V. Li, S.A. Barannikova, L.B. Zuev, The effect of hydrogen embrittlement on the mechanical properties of aluminum alloy, IOP Conf. Ser. Mater. Sci. Eng. 71 (2015) 12057, https://doi.org/10.1088/1757-899x/71/1/012057.
[103] Y.L. Liu, Y. Zhang, H.B. Zhou, G.H. Lu, F. Liu, G.N. Luo, Vacancy trapping mechanism for hydrogen bubble formation in metal, Phys. Rev. B 79 (2009), 172103, https://doi.org/10.1103/PhysRevB.79.172103.
[104] R.M. Nieminen, J. Laakkonen, Positron trapping rate into vacancy clusters, Appl. Phys. 20 (1979) 181–184, https://doi.org/10.1007/BF00885942.